# Transcriptome profiling of tendon fibroblasts at the onset of embryonic muscle contraction reveals novel force-responsive genes

Pavan Nayak[1], Arul Subramanian[2] and Thomas Schilling[2,3]

[1]Center for Complex Biological Systems, University of California Irvine, Irvine, CA

[2]Department of Developmental and Cell Biology, University of California Irvine, Irvine, CA

[3]Lead Contact

Author for Correspondence: Thomas F. Schilling, 4109 Natural Sciences II, Department of Developmental and Cell Biology, University of California Irvine, Irvine, CA 92617. Email: tschilli@uci.edu.

# Abstract

All cells are exposed to mechanical forces and must adapt to their physical environments but the underlying adaptive mechanisms remain unclear. To address this in developing tendons exposed to the extreme forces of muscle contraction, we have performed transcriptomics with tendon fibroblasts (tenocytes) isolated from zebrafish embryos before and after they start to swim. We find upregulation of known tenocyte markers as well as dramatic changes in expression of many novel tendon-associated genes. By paralyzing and restoring muscle contractions in embryos in vivo, we show that three of these novel genes, ECM proteins Matrix Remodeling Associated 5b (*mxra5b)* and Matrilin 1 (*matn1)*, as well as the transcription factor Kruppel-like factor 2a *(klf2a),* are force-responsive. In situ hybridization validates tendon-specific expression of all three genes. Quantitation using in situ hybridization chain reaction reveals that their transcript levels change specifically in subsets of tenocytes in response to force. These findings provide insights into force-dependent feedback mechanisms in tendons, which have important implications for improved treatments for tendon disease, injury and atrophy.

# Introduction

Cells experience mechanical forces from their environments such as adhesive interactions between adjacent epithelial cells or with the surrounding extracellular matrix (ECM). A key question is how cells adapt and respond to force through mechano-sensitive biochemical cell-signaling pathways. Force-responsive cellular mechanisms have been implicated in many aspects of cell differentiation **(D'Angelo, et al. 2011),** morphogenesis **(Keller et al. 2008; Hamada 2015)**, maintenance and repair **(Riley et al. 2022; Zhang et al., 2022)**. Despite their importance, these mechanisms remain understudied in vivo, particularly those that involve cell-ECM interactions. Dramatic examples of such interactions occur in tendons and ligaments of the vertebrate musculoskeletal system. Tendons experience a broad range of contractile forces from muscles, such as the extreme compressive forces on the human Achilles tendon during exercise, and constantly remodel themselves and their surrounding ECM to adapt **(Wang, 2005; Subramanian and Schilling, 2015)**. Tendon injuries and atrophy with aging are very common and a better understanding of the roles played by force in tendon development will aid in developing effective treatments.

Tendons are ECM-rich structures that connect muscles to cartilages and bones. The highly coordinated events leading to the proper formation of these connections in vertebrates relies upon cell-ECM interactions **(Schweitzer et al., 2010; Subramanian and Schilling, 2015)**. For example, in the early embryonic zebrafish trunk, myotendinous junctions (MTJs) develop via distinct tendon-independent and tendon-dependent stages of attachment. Differentiating myoblasts first secrete ECM proteins such as the integrin ligands Thrombospondin-4 (Tsp4) and Laminin-2 (Lama2) into the developing "pre-tendon" ECM, which establishes a rudimentary attachment, after which tenocyte progenitor cells (TPC) migrate to the site leading to MTJ maturation **(Subramanian et al., 2014)**. Tenocytes also extend long microtubule-rich projections outwards into the surrounding ECM, with which they may respond to mechanical force to locally regulate ECM composition **(McNeilly et al., 1996; Pingel et al., 2014;**

**Subramanian et al., 2018)**. The maturation of myoblasts and subsequent contractile forces acting on the MTJs activate Transforming Growth Factor β (TGF-β) coupled, phospho-SMAD (pSMAD)-dependent signaling in TPCs **(Pryce et al., 2009; Berthet et al., 2013)**. Although TGF-β is not necessary for TPC specification, it induces expression of the transcription factors Scleraxis (Scx) and Mohawk (Mkx), likely through Smad3 binding, which drive tenocyte fate by directly promoting transcription of tendon-specific ECM proteins, such as Collagen 1 (Col1a1, Col1a2), Col12a1 and Col14 as well as Matrix Metalloproteinases (MMPs) involved in ECM remodeling **(Berthet et al., 2013; Maeda et al., 2011; Rullman et al., 2009)**. TGF-β signaling via Smad3 and/or Mkx also represses genes involved in myogenic and skeletogenic fates, such as *MyoD* **(Chuang et al., 2014; Liu et al., 2001)**, *Sox6* **(Anderson et al., 2012)** and *Runx2* **(Kang et al., 2005)**.

Cell type and matrix composition differ along the length of many tendons to aid in load bearing and force transmission. For example, the enthesis region where a tendon attaches to bone is structurally composed of a gradient of stiffer fibrocartilage closer to the attachment. This is thought to help transfer mechanical stress between the elastic tendon tissue and rigid bony matrix **(Lu and Thomopoulos, 2013)**. Attachment cells along this fibrocartilage co-express Scx and Sox9, which likely contributes to the specialized enthesis ECM structure **(Blitz et al., 2013) (Zelzer et al., 2014)**. Dysregulation of force in tendons leads to changes in collagen fibril size and organization **(Pingel et al., 2014)**, as well as levels of *COL1*, *COL3*, and *MMP3* mRNA **(Ireland et al., 2001)**. Force-responsive tenocyte mRNA expression profiles have been examined in vitro and ex vivo following injury and during repair. However, while many studies have demonstrated effects of force on tenocyte transcription in vitro, there have been no comprehensive transcriptomic studies of tenocyte responses to force in vivo, especially during embryonic development and the onset of muscular contraction. We have previously shown that force resulting from the onset of embryonic muscular contraction is required for proper tendon maturation in zebrafish embryos, including tenocyte morphogenesis and ECM production **(Subramanian et al., 2018)**.

Here we perform genome-wide bulk RNA-sequencing (RNA-seq) on FAC-sorted tenocytes of developing zebrafish embryos during the onset of active swimming and trunk muscle contraction. We identify several known tenocyte markers, expression of which is upregulated as tendons differentiate, as well as numerous other up- or downregulated genes about which relatively little is known in the context of tenocyte development or mechano-transduction. Using genetic and physiological perturbations of muscular force in vivo, we show force-responsiveness of several of these novel tenocyte-associated genes. These include genes encoding two ECM proteins, Matrix Remodeling Associated 5b (*mxra5b)* and Matrilin 1 (*matn1)*, as well as the transcription factor Kruppel-like factor 2a *(klf2a).* We further use quantitative in situ methods to confirm their tenocyte- and enthesis-specific expression as well as their force-responses. These findings provide insights into force-dependent feedback mechanisms in tendons, which have important implications for improved treatments for tendon disease, injury and atrophy.

# Results

## Onset of active muscle contraction alters tenocyte gene expression

Previously, we showed that tenocytes in trunk muscle attachments undergo distinct morphological transformations coinciding with the onset of muscle contraction **(Subramanian et al., 2018)**. Since these changes occur during the embryonic transition from twitching (36 hours post-fertilization, hpf) to free-swimming behavior (48 hpf), we hypothesized that force-induced transcriptional changes in tenocytes underlie these morphological changes. To test this and identify potential force-responsive factors, we conducted RNA-seq with FAC-sorted populations of *Tg*(*scxa:mCherry)*-positive tenocytes isolated from dissociated 36 or 48 hpf embryos. From 11 total biological replicates (7 replicates for 36 hpf, 4 replicates for 48 hpf after quality control **(see Methods)**, 35 embryos per replicate) we obtained approximately 10,000-15,000 cells per sample replicate. Pair-wise comparisons of over 17,000 genes from bar-coded cDNA libraries revealed 1,123 differentially expressed genes (DEGs) between 36 and 48 hpf with a False Discovery Ratio (FDR) adjusted p-value < 0.05 **(Fig. 1A).** These included upregulation of known tenocyte markers such as *tnmd, mkxa,* and *egr1* **(Fig. 1B),** confirming that the sorted mCherry positive cells included mature tenocytes or progenitors in the process of differentiation. *scxa* expression also increased, though with a slightly less significant adjusted p-value (0.09) **(Supplementary Data 1)**. Principle Components (PC) associated with biological replicates segregated according to experimental condition (36 versus 48 hpf), validating the library preparation protocol **(Fig. 1C)**. GO analysis for Biological Process (BP) terms associated with the top DEGs showed significant enrichment for “skeletal system development” and “ECM organization” **(Fig 1D)**, while Molecular Function (MF) and Cellular Component (CC) GO terms were similarly enriched for ECM-associated features **(Supplementary Figure 1)**. Surprisingly, among the DEGs were genes typically associated with cartilage development and morphogenesis, including *matn1*, *col2a1a* and *col9a1a.* This suggests novel roles for these genes in

tenocytes, possibly an early subset of *scxa+* cells in embryonic tendons that have already adopted a fibrocartilage fate later associated with developing entheses.

To identify cell signaling and cell adhesion pathways implicated in force-responses during embryonic tendon development, we analyzed our DEG list using two software suites, PANTHER **(Mi and Thomas, 2019) (Supplementary Table 1)** and DAVID **(Supplementary Table 2)**, which utilize KEGG pathway annotations, for pathway analysis **(Huang et al., 2009)**. PANTHER identified DEGs associated with 96 different pathways, including many genes implicated in Wnt, TGF-β, Platelet Derived Growth Factor (PDGF), and Retinoic Acid (RA) signaling as well as Integrin (Itg) and Cadherin (Cdh) mediated adhesion **(Supplementary Table 1).** In contrast, DAVID identified DEGs involved in RA metabolism, an emerging pathway of interest in tendon development, and also highlighted differential expression of genes encoding many ribosomal proteins. **(Supplementary Table 2)**.

Our RNA-seq DEG datasets were obtained from TPCs and tenocytes during the onset of swimming, so we performed a targeted search for DEGs associated with mechanosensitive pathways, which might have been missed by pathway analysis software due to limitations in annotation databases. Using a custom automated literature screening tool, LitScreen **(see Methods)**, three genes of particular interest, *matn1*, *klf2a* and *mxra5b,* emerged based either on their force-dependent regulation in other biological contexts, and/or regulation by TGF-β, a well-known force-responsive signal. *matn1,* which encodes an ECM protein highly enriched in cartilage, was the top-most upregulated gene by FDR adjusted p-value **(Supplementary Data 1)**. Matn1 has been implicated in enhancement of chondrogenesis of synovial fibroblasts treated with TGF-β **(Pei et al. 2008)**. The transcription factor *klf2a* was also strongly upregulated and Klf proteins such as Klf2 and Klf4 have been implicated in enthesis development in mammalian tendons **(Kult et al., 2021).** Klf proteins repress TGF-β signaling in endothelial cells **(Boon et al., 2007; Li et al., 2021)** and *klf2a* expression is mechanosensitive during heart valve development **(Steed et al., 2016).** *mxra5b* encodes an ECM protein expressed in both

tendons and ligaments during chick development **(Robins and Capehart, 2018)** and is regulated by TGF-β signaling in cultured human kidney epithelial cells **(Poveda et al., 2017**). Other potential mechanosensitive genes in our RNA-seq dataset based on literature screening for pathways "Piezo" and "YAP/TAZ", included *her2* and *ccn1,* respectively. Interestingly, *her2* expression increases in response to force in gastric cancer cells **(Akutagawa et al., 2018)**, and *ccn1 (*also known as *cyr61)* is expressed in limb tendons in mice **(Lorda-Diez et al., 2011).** For these reasons, we focused on *matn1*, *klf2a* and *mxra5b* for further analysis.

### ***matn1*, *klf2a* and *mxra5b* are expressed in tenocytes and respond to perturbations of muscular contraction in vivo**

To verify specific expression of *matn1*, *klf2a* and *mxra5b* in tenocytes, we performed in situ hybridization (ISH). Conventional chromogenic ISH for *matn1* failed to detect expression at 36 hpf, whereas strong expression was observed at 48 and 60 hpf in developing craniofacial and pectoral fin cartilages **(Fig. 2A-C)**. Because of its strong expression in chondrocytes, we hypothesized that differential expression of *matn1* in our dataset could be a result of tenocyte-specific expression in developing enthesis progenitors closely associated with embryonic cartilages. To this end, we conducted double fluorescent in situ Hybridization Chain Reaction (*is*HCR) for *scxa* and *matn1* at 51 hpf, 3 hours older than our RNA-seq samples to allow better visualization of differentiated chondrocytes, and 72 hpf. We found co-expressing cells at the ceratohyal-interhyal (ch-ih) and ceratohyal-hyohyal (ch-hh) cartilage-muscle attachment sites at 72 hpf **(Fig. 3A-E Supplementary Figure 2A-G)**. For *klf2a,* chromogenic ISH revealed expression at somite boundaries in the trunk at 48 hpf as well as developing pharyngeal arches and pectoral fins at 48 and 60 hpf **(Fig. 2D-F)**. This was confirmed by double *is*HCR of *klf2a* and *scxa* showing overlapping expression in tenocytes at somite boundaries at 48 hpf **(Figure 3F-J)**. *mxra5b* expression was

first detected at somite boundaries near the horizontal myoseptum (HMS), which separates dorsal and ventral somites at 36 hpf, as well as in the notochord at 48 hpf. Expression increased and extended along the somite boundaries by 60 hpf at trunk muscle-tendon attachment sites (**Fig. 2G-I**). Using double isHCR of *scxa* and *mxra5b,* we found co-expressing tenocytes at somite-boundaries in embryos at 48 hpf and 72 hpf **(Fig. 3K-O)**.

Because *matn1, klf2a* and *mxra5b* were identified among the top DEGs at the onset of swimming behavior **(Supplementary Data 1; Fig 4A-C)**, we hypothesized that mechanical force may regulate their expression. To test this, we performed Real Time Quantitative-PCR (RT-qPCR) in genetically paralyzed embryos. Relative expression of each gene was compared between wild-type (WT) embryos and homozygous mutants for voltage dependent L-type calcium channel subtype beta-1 (*cacnb1*$^{-/-}$), which are paralyzed due to lack of muscle contraction **(Subramanian et al., 2018; Zhou et al., 2006)**. At 48 hpf, we observed significant downregulation of all 3 genes in *cacnb1*$^{-/-}$ mutants as compared to WT **(Fig. 4D).** In contrast, at 72 hpf, only *matn1* and *mxra5b* remained downregulated, while *klf2a* expression increased in paralyzed embryos **(Fig. 4E)**. To confirm that these expression changes are due to loss of mechanical force, we injected embryos at the 1-cell stage with mRNA encoding full-length alpha-bungarotoxin mRNA (αBTX), which irreversibly binds to acetyl choline receptors at the neuromuscular synapse leading to paralysis. We used 90ng/ul of full-length αBTX mRNA which was optimized to paralyze embryos for the first two days of embryogenesis after which they gradually recover movement. A proportion of αBTX-injected (αBTX-inj) embryos regained muscle contractions at 48 hpf and we performed RT-qPCR on cDNA derived from control, αBTX-inj paralyzed, and αBTX-inj recovered embryos. We separated 48 hpf recovered embryos into two subgroups based on the extent of muscle contraction: 1) partially recovered (Twitching), in which embryos showed sporadic contractions of the trunk and pectoral fin muscles, but did not swim freely, similar to embryos at 36 hpf and 2) fully recovered (Recovered), in which embryos swam freely. At 48 hpf, RT-qPCR revealed

significant downregulation of *matn1* and *mxra5b* in αBTX paralyzed embryos compared to WT uninjected siblings, similar to the relative expression we observed in *cacnb1*$^{-/-}$ mutant embryos **(Fig. 4F)**. *matn1* and *mxra5b* were upregulated in twitching and recovered embryos, though these results were not statistically significant for *mxra5b* (**Fig. 4G, H**). In contrast, *klf2a* was upregulated, though not statistically significantly, in paralyzed embryos versus WT embryos **(Fig. 4F)**. These results, combined with our RNA-seq findings, suggest that *matn1, klf2a,* and *mxra5b* transcription are regulated by the mechanical forces of muscle contraction.

**Tenocyte-specific gene expression of *klf2a*, *mxra5b* and *matn1* is regulated by muscle contraction**

Because RT-qPCR was performed on cDNA isolated from whole embryos rather than on tenocytes alone, the expression differences we observed for *matn1, klf2a*, and *mxra5b* may have reflected changes in expression in cell types other than tenocytes (e.g. *matn1* in cartilage). Therefore, to confirm force-responsiveness in tenocytes, we examined expression of *matn1, klf2a*, and *mxra5b* in *scxa*-positive cells at 48 or 72 hpf by *is*HCR, using our αBTX paralysis-recovery experimental protocol **(Fig. 4I-K)**. For *matn1*, we quantified expression by measuring its fluorescence intensity in individual attachment cells at the ch-ih and ch-hh attachment sites of the distal end of the ch cartilage. Individual attachment cells were carefully selected for quantification only if they satisfied the following criteria: 1) they were located at these muscle attachment sites, 2) they co-expressed both *matn1* and *scxa* and 3) they were spatially adjacent to both chondrocytes expressing high levels of *matn1* alone and tenocytes expressing high levels of *scxa* alone. Individual cell quantification revealed no significant difference in *matn1* expression between WT and paralyzed embryos, but a drastic increase in expression in partially recovered, twitching embryos, followed by a return to WT levels in fully recovered embryos **(Fig. 4I)**. For *mxra5b* quantification, we examined its fluorescence intensity in *scxa/mxra5b* double positive tenocytes located

at somite boundaries at 48 hpf. Individual cells were selected for analysis only if they were located along ventral somite boundaries or HMS regions and co-expressed *scxa* and *mxra5b*. Similarly, for *klf2a*, we quantified expression by measuring its fluorescence intensity in *scxa*/*klf2a* double positive tenocytes at the somite boundaries, primarily at the HMS. We observed increased expression of *klf2a* in paralyzed embryos compared to WT, then a return to WT levels upon full recovery **(Fig. 4J)**. Conversely, we observed decreased expression of *mxra5b* in paralyzed embryos compared to WT, followed by a return to WT levels in twitching and recovered groups **(Fig. 4K)**. Together, these results suggest that mechanical force initiated by the onset of muscle contraction regulates the transcriptional dynamics of *matn1* in cartilage attachment cells of craniofacial tendons, which are putative enthesis progenitors, as well as *klf2a* and *mxra5b* in tenocytes associated with axial and trunk muscle attachments.

# Discussion

Whereas mechanotransduction has been implicated in tenocyte development and tendon maintenance, few studies have examined transcriptional changes within these fibroblasts in response to force, particularly in vivo. Here, we provide a genome-wide profile of differential tenocyte gene expression during critical stages of muscle contraction onset and differentiation of TPCs in zebrafish embryos. We identify three force-responsive genes, two encoding ECM proteins, *matn1* and *mxra5b,* and one transcription factor, *klf2a,* and show that perturbing muscle contraction alters their mRNA levels specifically in tenocytes. While *matn1* expression appears specific to entheseal tenocytes at cranial muscle attachments to cartilage involved in jaw movements, *mxra5b* and *klf2a* expression localizes to tenocytes associated with MTJs of the axial musculature involved in swimming **(Figure 5)**. These results are consistent with a model in which tenocytes continuously sense force and respond by altering transcription of genes involved in fine tuning the surrounding ECM **(Subramanian and Schilling, 2015; Subramanian et al., 2018)**. Many tendon mechanotransduction studies have been performed with mature tendons in in vitro/ex vivo conditions e.g. explanted into collagen matrices and exposed to cyclical strain or other forces. Our results demonstrate transcriptional changes in developing tenocytes in response to force in vivo in intact embryos when tendons first form and identify novel components of tenogenesis. They also highlight the close relationship between genes implicated in cartilage (i.e. *matn1*) and fibrocartilage (i.e. *KLF* transcription factors) associated with tendon entheses with tenocytes and their coordinated responses to mechanical force.

Though typically thought of as cartilage-specific ECM proteins, expression of matrilin genes, including Matn1, has been reported in single-cell RNA-seq (scRNA-seq) analyses of newly differentiating tendon and fibrocartilage fibroblasts **(Kaji et al., 2021)**. Our results confirm *matn1* expression in zebrafish tenocytes at muscle attachments immediately adjacent to cartilage in situ, consistent with developing entheses, and demonstrate an acute response to mechanotransduction. Our RT-qPCR data

show decreased *matn1* expression in whole embryos in the absence of muscle contraction. However, expression in cranial tenocytes as detected by isHCR remains unchanged under the same conditions and then rapidly increases as the embryo recovers from paralysis. This may be due to differential responses in cartilage-specific versus tendo-chondral expression to muscle contraction force. In mammals, Matn1 is essential for ECM organization in cartilage, as chondrocytes and their surrounding ECM are disorganized in *Matn1*$^{-/-}$ mutant mice and expression returns when mechanical load is restored during recovery from medial meniscus destabilization surgery **(Chen et al., 2016)**. Ours are the first studies implicating Matn1 in tendon/fibrocartilage development or mechanotransduction. Similarities in mechanosensitive expression in chondrocytes and tenocytes associated with muscle attachments suggest that Matn1 may function in establishment/organization of the ECM stiffness gradient between stiffer cartilage and more flexible tendon at the enthesis.

*Mxra5* (also known as *adlican*) encodes a secreted proteoglycan implicated in cell-cell adhesion and/or ECM remodeling as shown in the pathological context of cancer **(He et al., 2015) (Wang et al., 2013)**. We provide evidence that *mxra5* expression in axial tenocytes involved in swimming requires the force of muscle contraction and is rapidly upregulated in response to the recovery of force following paralysis. *MXRA5* expression has been reported in tendons and connective tissues of developing chick embryos **(Robins and Capehart, 2018)**, but its functions remain unclear. Human *MXRA5* is also expressed in fibroblasts **(Chondrogianni et al., 2004)**, upregulated along with other ECM-associated genes in response to injury **(Gabrielsen et al., 2007)**, and downregulated in response to TGF-β1 **(Poveda et al., 2017)** in various tissue contexts**.** Our results provide some of the first evidence that *mxra5* is a mechanosensitive gene, possibly regulated by TGF-β. However, while our RT-qPCR results suggest that *mxra5* is downregulated upon muscle contraction, both RT-qPCR and *is*HCR results show *mxra5* upregulation upon recovery from paralysis. This apparent discrepancy may reflect differences in the cell populations sampled (e.g. whole embryos versus tenocytes), or more interestingly may reflect other

developmental regulators of *mxra5b* acting in parallel to mechanotransduction in tenocytes. For example, tenocytes may acquire a temporary ECM remodeling state in *cacnb1*$^{-/-}$ mutant and αBtx-injected embryos associated with increased expression of *Mxra5* as suggested for pathologies such as myocardial ischemia **(Gabrielsen et al., 2007)** or osteoarthritis **(Balakrishnan et al., 2014)**. Further studies will be required to delineate functional roles for Mxra5 in vertebrate tenocytes.

Recent research in mice showed roles for KLF2, as well as KLF4, in cell differentiation at tendon-bone entheses **(Kult et al., 2021)**, but did not explore their responses to force. We show that *klf2a* in zebrafish axial tenocytes is mechanoresponsive. While αBTX-injected embryos showed no significant changes in *klf2a* expression with paralysis, it was significantly downregulated in tenocytes upon recovery **(Fig. 4F, 4J)**. In contrast our RNA-seq data showed *klf2a* upregulation with onset of muscle contraction **(Fig. 4B)**. Like *mxra5*, these apparent discrepancies may reflect distinct cell populations sampled or separate parallel pathways that regulate *klf2a*. Although *Klf2* is regulated by force in other contexts, such as endocardial and vascular endothelial cells **(Lee et al., 2006; Boselli et al., 2015; Steed et al., 2016),** the molecular pathways that control *Klf2* expression are not well characterized.

We found dramatic changes in expression of many other genes implicated in crucial developmental and mechanotransduction signaling pathways that appear differentially expressed in response to muscle contraction in zebrafish tenocytes. These include well studied pathways such as TGF-β, as well as others such as and RA, Piezo and YAP/TAZ signaling, about which roles in tenocytes remain largely unexplored. Recent research in mammals has implicated RA-signaling in tendon development **(Mcgurk et al., 2017)**, including tenocyte fate determination and TGF-β signaling **(Kaji et al., 2021)**. The RA degradation enzyme *cyp26b1* has also been implicated in cranial tendon development in zebrafish **(Supplementary Data 1) (Laue et al., 2008)**. Two genes implicated in the Piezo mechanotransduction pathway, *her2* and *atf2,* were both downregulated upon onset of muscle contraction in our DEG dataset

**(Supplementary Data 1)**. Piezo 2 regulates *her2* expression in breast cancer cells **(Lou et al., 2018)**, while PIEZO1 regulates *atf2* in chondrocytes **(Lee et al., 2021)**. Finally, a gene shown to be regulated by the YAP-TAZ mechanotransduction pathway, *CCN1,* was upregulated upon onset of muscle contraction in our RNA-seq data **(Supplementary Data 1) (Ho et al., 2018)**. Recent studies suggest that tenocytes cultured in a 3D collagen matrix and subjected to mechanical uniaxial stretching upregulate *Yap1* **(Kaji et al. 2021).** Our data provide further support for roles for RA signaling as well as Piezo and Yap/Taz mediated mechanotransduction in tenocytes and suggest that their functions are conserved in zebrafish.

TGF-β signaling is a well-established regulator of tenocyte cell fate **(Subramanian and Schilling, 2015; Bobzin et al., 2021)**, but the gene regulatory networks acting up- or downstream of this signal remain largely unknown in a force-response context. Of the three force-responsive genes we have implicated in tenocyte development, relatives of two of them, *mxra5b,* and *klf2a,* have been linked to TGF-β signaling. Human MXRA5 is downregulated in response to TGF-β1 in the context of inflammation and fibrosis **(Poveda et al., 2017).** Several KLF proteins, including KLF2, have been implicated in TGF-β signaling in various tissue types **(Boon et al., 2007; Li et al., 2021; Memon et al., 2018).**

Our analyses of *matn1, mxra5a* and *klf2a* also hint at specific roles in different subpopulations of tenocytes subjected to different forces. While *matn1* is expressed in entheseal tenocytes associated with cartilage, *mxr5a* and *klf2a* expression localizes to tenocytes in the MTJs of axial muscles. We therefore propose a model in which expression of tenocyte marker genes respond distinctly to varying muscle contraction force conditions **(Figure 5A-5C)**. In the developing jaw entheses tenocytes increase *matn1* expression acutely upon sensing of intermittent/acute contraction force (i.e sporadic jaw contraction during cranial tendon development) **(Figure 5B)**. Conversely, the tenocytes of developing trunk MTJs bear the stress of two different contraction conditions: intermittent sporadic trunk contraction forces such as those observed during 36 hpf embryos or during “Twitching” recovery of muscle contraction from αBtx-injection induced paralysis, and continuous contractions, such as those

306 required during maintenance of posture along the anteroposterior axis. Trunk MTJ tenocytes
307 downregulate *klf2a* expression in both intermittent and continuous force conditions, whereas *mxra5b*
308 expression is increased in only continuous force conditions **(Figure 5A, 5C)**. These contextual differences
309 in force-response may reflect the intricate nature of fine-tuning spatially distinct tendon ECM structures
310 and functions during diverse biological processes like development, maintenance and repair. To address
311 functions of these genes we have used CRISPR/Cas9 mutagenesis to generate F0 Crispants for *matn1*,
312 *klf2a* and *mxra5b*, but have not observed any obvious phenotypic defects, possibly due to genetic
313 redundancy with other similar proteins, or compensation. Generating stable mutant lines and testing
314 their requirements in tenocytes such as changes in response to varying mechanical forces (Schilling and
315 Subramanian, 2014) is an important avenue of future study.

316 Whereas bulk RNA sequencing strategies such as those performed here provide deeper read
317 depth for identification of sparsely expressed genes, they may miss critical cell types and specific
318 expression patterns necessary to interpret complex processes occurring in tendons during
319 morphogenesis. Single-cell approaches (e.g. scRNA-seq) at different developmental stages and in the
320 presence or absence of force, will provide a clearer understanding of how individual cells and cell
321 populations respond to force in development. Integrating such knowledge of the basic biology of
322 tenocytes at multiple scales will be essential for optimizing translational therapies in the future.

323

# 324 Figure Legends

325 **Figure 1: Genes differentially expressed in tendon progenitor cells upon onset of embryonic muscle**
326 **contraction**

**A)** Heatmap from bulk RNA-seq of FAC-sorted *scxa:mCherry+* tenocytes displaying 1,123 genes differentially expressed between 36 hpf and 48 hpf. FDR adjusted $p < 0.05$. **B)** Elevated expression of tenocyte marker genes *mkxa, tnmd,* and *egr1* in RNA-seq experiments at 48 hpf. Datapoints represent normalized read counts of single biological replicates for each color-coded timepoint (n=7 for 36 hpf, n=4 for 48 hpf). **C)** PCAs of individual replicates showing separation of experimental conditions by timepoint. **D)** GO analysis using Biological Process (BP) terms of top 1,123 differentially expressed genes (DEGs) by adjusted p-value.

**Figure 2: Embryonic expression of novel tenocyte progenitor markers**

Expression of *matn1, klf2a* and *mxra5b* mRNA detected by whole mount ISH. **(A-C)** *matn1* expression in skeletal progenitors at 48 hpf **(A)** and in pharyngeal, neurocranial and pectoral fin cartilages (and associated tenocytes) at 60 hpf **(B,C)**. **(A,B)** Lateral views. **(C)** Ventral view. **(D-F)** *klf2a* expression in pharyngeal mesenchyme at 36 hpf **(D)**, skeletal progenitors and in tenocytes along somite boundaries (sb) at 48 and 60 hpf **(E,F)**. Lateral views. **(G-I)** *mxra5b* expression in tenocytes along somite boundaries and the notochord at 36, 48 and 60 hpf. Scale bars = 100µm. Abbreviations: abc = anterior basicranial commissure, ch = ceratohyal cartilage, ep = ethmoid plate, hs = hyosymplectic cartilage, mc = meckel's cartilage, nc = notochord, pf = pectoral fin, pq = palatoquadrate cartilage, sb = somite boundaries, t = trabeculae cartilage.

**Figure 3: Co-expression of *matn1, klf2a* and *mxra5b* with *scxa* in tenocytes**

Expression of *matn1, klf2a,* and *mxra5b* (green) and *scxa* (red) detected by whole mount *is*HCR. **(A-E)** *matn1* co-localizes with *scxa* at muscle attachment sites on developing pharyngeal cartilages at 72 hpf.

Ventral view, anterior to the left. (**D, E)** Higher magnification confocal images of the lower and upper dashed boxes in **A,** respectively. **(F-H)** *klf2a* co-localizes with *scxa* at somite boundaries at 48 hpf. Lateral views, anterior to the left. **(I, J)** Higher magnification confocal images of somite boundaries regions indicated by left and right dashed boxes in **(F)**. **(K-M)** *mxra5b* co-localizes with *scxa* at somite boundaries, particularly along the horizontal myoseptum, at 48 hpf. Lateral views, anterior to the left. **(N**, **O)** Higher magnification confocal images of somite boundaries of left and right dashed boxes in **K**. Abbreviations: ch = ceratohyal cartilage, ch-ih (a) = anterior ceratohyal-interhyal attachment , ch-ih (p) = posterior ceratohyal-interhyal attachment, ch-hh = ceratohyal-hyohyal attachment, HMS = horizontal myoseptum, hs = hyosymplectic cartilage, mc = meckels cartilage, pq = palatoquadrate cartilage, sb = somite boundaries, sv = segmental blood vessels. Arrowheads and dashed circles in **D, E, I, J, N, O** indicate examples of co-expressing cells from which individual cell substacks were quantified**.** Scale bars = 50µm

**Figure 4: Expression dynamics of *matn1, klf2a,* and *mxra5b* in response to force perturbations**

**(A-C)** Plots of *matn1*, *klf2a*, and *mxra5b n*ormalized read counts from RNA-seq at the onset of zebrafish active muscle contraction at 36 hpf (red) and at 48 hpf (blue). Each point represents a single biological replicate. **(D, E)** Histograms quantifying RT-qPCR data from WT control (blue bars) and *cacnb1*$^{-/-}$ mutants (red bars) at 48 hpf **(D)** and 72hpf **(E)**. RT-qPCR of *matn1*, *klf2a*, and *mxra5b* in uninjected WT controls (blue bars) and αBtx-injected paralyzed (green bars) embryos at 48 hpf **(F)**, in αBtx-injected paralyzed (green bars) and αBtx-injected "Twitching" (partially recovered, magenta bars) embryos at 48 hpf **(G)**, and in WT controls (green bars) and αBtx-injected, "Recovered" (blue bars) embryos at 48 hpf **(H)**. **(I-K)** Box plots of fluorescence intensity/area measurements from individual cell confocal substacks labeled for *matn1 /scxa* **(I)**, *klf2a/scxa* **(J)** and *mxra5b/scxa* **(K)** RNA with *is*HCR in WT controls (red), αBtx-

372 injected, paralyzed (green), twitching (blue) and recovered (magenta) embryos at 72hpf. By gene and
373 condition, the sample numbers are as follows: for *matn1*, WT: n = 3 embryos, 30 cells; Paralyzed: n= 4
374 embryos, 30 cells; Twitching: n = 5 embryos, 40 cells; Recovered: 3 embryos, 30 cells; For *klf2a*, WT: n =
375 5 embryos, 39 cells; Paralyzed: n= 6 embryos, 20 cells; Twitching: n = 5 embryos, 33 cells; Recovered: 3
376 embryos, 15 cells; For *mxra5b*, WT: n = 3 embryos, 30 cells; Paralyzed: n= 4 embryos, 40 cells;
377 Twitching: n = 4 embryos, 40 cells; Recovered: 4 embryos, 40 cells. ns = not significant, * $p < 0.05$, ** $p <$
378 0.01, *** $p < 0.001$.

379 **Figure 5: Proposed model for context-specific expression patterns of *matn1, klf2a,* and *mxra5b* across**
380 **distinct tendon attachment regions.**

381 **A-B)** Tendons from spatially separate regions must undergo unique force conditions. Whereas cranial
382 jaw entheseal tenocytes may experience more acute forces from jaw contractions, tenocytes of the MTJ
383 may experience both acute and continuous forces from activities such as swimming and posture
384 maintenance respectively. **C)** Acute muscle contraction conditions cause upregulation of *matn1* in
385 entheseal tenocytes, whereas trunk MTJ tenocytes downregulate *klf2a* expression in acute and
386 continuous contraction conditions, while only upregulating *mxra5b* in continuous force conditions.

387 **Supplementary Table 1: Pathway list from differentially expressed genes using PANTHER**

388

389 **Supplementary Table 2: KEGG pathways analyzed from differentially expressed genes using DAVID**

390

391 **Supplementary Table 3: Primer sequences (5' -> 3') used for ISH and RT-qPCR**

392

**Supplementary Data 1: Differentially expressed genes from RNA-seq between 36 and 48 hpf**

Columns are as follows (standard DESeq2 output): baseMean = normalized count mean for all samples, Log2FoldChange = log2 fold change 36 hpf vs 48 hpf, lfcSE = standard error 36 hpf vs 48 hpf, stat = Wald statistic 36 hpf vs 48 hpf, pvalue = Wald test p-value, 36 hpf vs 48 hpf, padj = Benjamini Hochberg FDR adjusted p-value.

**Supplementary Figure 1: RNA-seq GO term analyses for Molecular Function (MF) and Cellular Compartment (CC) GO categories**

**A)** MF GO term analysis from 1,123 DEG list by FDR adj. p-value with $p < 0.05$. **B)** CC GO term analysis from top 1,123 DEG list by FDR adj. $p < 0.05$

**Supplementary Figure 2: *matn1* expression in the embryonic zebrafish craniofacial complex and associated tendons and muscles**

**(A-C)** *is*HCR for *matn1* (green) and *scxa* (red) in 51 hpf zebrafish embryos, ventral views, anterior to the left. (**D-G)** Immunolabeling for mCherry in *Tg*(*scxa:mCherry*;*sox10*:*GFP*) embryos (red, tendon), GFP (green, cartilage) and Myosin Heavy Chain (blue, muscle) at 72 hpf. White-dashed boxes depict ceratohyal-interhyal and ceratohyal-hyohyal attachment regions measured in *is*HCRs in **Fig. 4I**. Abbreviations: ch = ceratohyal cartilage, ch-ih (a) = anterior ceratohyal-interhyal attachment region, ch-ih (p) = posterior ceratohyal-interhyal attachment region, mc = meckel's cartilage, pq = palatoquadrate cartilage, Scale bars = 20um

# Methods

## Zebrafish embryos, transgenics and mutants

AB strain wild type, *TgBAC(scxa:mCherry)*$^{fb301}$ (referred to in this paper as *Tg(scxa:mCherry)*), or *cacnb1*-$^{ir1092/ir109}$*;fb301Tg* (referred to in this paper as *cacnb1*$^{-/-}$*)* transgenic zebrafish embryos were collected in natural matings, raised in embryo medium at 28.5°C **(Westerfield, 2007)** and staged as described **(Kimmel et al., 1995)**. Craniofacial musculoskeletal structures were identified as described (**Schilling and Kimmel, 1997)**. All protocols performed on embryos and adult zebrafish in this study had prior IACUC approval.

## In situ hybridization (ISH)

Antisense RNA probes for *matn1*, *klf2a*, and *mxra5b* were generated using T7 sequence-tagged primers **(Supplementary Table 3)** to amplify from cDNA, reverse transcribed using the ProtoScript II First Strand cDNA Synthesis Kit (NEB E6560), from 72 hpf WT embryos and synthesized using T7 RNA polymerase (Roche, 10881767001) and DIG RNA labelling mix (Roche, 11277073910). Whole-mount ISH was performed with anti-DIG-AP fragments (Roche, 11093274910) at 1:2000 dilution, as described in **Thisse et al., 1993**.

## In situ hybridization chain reaction (*is*HCR) and immunohistochemistry

*is*HCR probes were designed by Molecular Technologies (Los Angeles, CA) and whole mount *is*HCR was performed with amplifiers/probes obtained from Molecular Instruments according to the *is*HCR v3.0 protocol as described **(Choi et al., 2014)**. Probes/amplifier combinations used were: *matn1* (NCBI ref. # 403023) and *mxra5b* (NCBI ref. # 795448) in B1 with B1 Alexa Fluor 488, *scxa* (NCBI ref. # 100034489) in B2 with B2 Alexa Fluor 546, *klf2a* (NCBI ref. # 117508) in B3 with B3 Alexa Fluor 647. Whole embryo immunohistochemistry was performed as described in **Subramanian et al., 2018**. Primary antibodies

used: rat monoclonal anti-mCherry (Molecular Probes − 1:500 dilution, M11217), chicken anti-GFP (Abcam – 1:1000 dilution, ab13970), mouse anti-myosin heavy chain (MHC) (Developmental Hybridoma - 1:250, A1025). Secondary antibodies used: Alexa Fluor 594 conjugated donkey anti-rat IgG (Jackson ImmunoResearch – 1:1000 dilution, 712-586-153), Alexa Fluor 488 conjugated donkey anti-chicken IgY (Jackson Immunoresearch, 1:1000 dilution, 703-486-155), Alexa Fluor 647 conjugated donkey anti-mouse IgG (Jackson Immunoresearch, 1:1000 dilution, 715-606-151).

## Collagenase dissociation and FACS sorting

Transgenic *Tg*(*scxa:mCherry*) zebrafish embryos were dissociated using collagenase IV (Roche, 17104019) at a concentration of 6.25 mg/ml without trypsin addition at a temperature of 28C for roughly 40 minutes, homogenizing every 5 min using a P1000 pipette. Cells were then filtered through a 40µm filter (Pluriselect-usa, 43-10040-50). Dissociated cell suspensions were sorted on a Bio-Rad FACS Aria II cell sorter. mCherry-positive cells were gated and sorted for those expressing at high levels.

## Bulk RNA-seq library preparation and sequencing

An RNEasy Micro Kit (Qiagen, 74004) was used for RNA extraction of cell lysates from FAC-sorted cells. RNA quality was checked at the UC Irvine Genomics High Throughput Facility (GHTF) using a Bioanalyzer 2100 Instrument (Agilent). Biological replicates with RNA Integrity Number (RIN) > 7 were used for library construction and sequencing. The Smart-seq2 protocol was utilized for cDNA library construction **(Picelli et al. 2014)**. Libraries were sequenced at the GHTF using a HiSeq 4000 sequencer (Illumina) at a read depth of ~35M reads per replicate.

## Bulk RNA-seq data analysis

Reads were mapped to zebrafish genome version GRCz10 and quantified using STAR v2.5.2a **(Dobin et al. 2013)** and RSEM v1.2.31 **(Li and Dewey 2011)**. Differential gene expression analysis and PCA were

459 performed using R package DESeq2 v1.30.1. Pairwise comparisons were performed between 36 hpf and
460 48 hpf sorted tenocytes, and a Benjamini-Hochberg FDR adjusted p-value < 0.05 was used as a threshold
461 for considering significant differences in gene expression levels. PCA was performed on normalized
462 count data which underwent variance-stabilization-transformation using DESeq2. Heatmaps were
463 generated using ClustVis **(Metsalu and Vilo, 2015)**. GO term enrichment analysis was performed using
464 the ClusterProfiler R package **(Wu et al., 2021).** In GO term plots, Gene Ratios are described as *k/n*
465 where *k* is the number of genes from the input list of DEGs mapping to the given GO term and *n* is the
466 total number of input genes mapping to any GO term.

467 **αBTX injections**

468 αBTX mRNA was synthesized from the *Pmtb-t7-alpha-bungarotoxin* vector (Megason lab, Addgene,
469 69542) as described in **Swinburne et al. 2015** and injected into embryos at the 1-cell stage at a volume
470 of 500 picoliters per embryo. αBTX mRNA was injected at a concentration of 90 ng/µl to paralyze
471 embryos that were collected at 48 hpf and 150 ng/µl to paralyze embryos that were collected at 72 hpf.

472 **RT-qPCR**

473 Wild type, *cacnb1*$^{-/-}$, αBtx-paralyzed, twitching, and recovered embryos were collected at respective
474 timepoints, homogenized in Trizol with prefilled tube kits using high impact zirconium beads
475 (Benchmark Scientific, D1032-10) using a BeadBug 3 Microtube Homogenizer D1030 (Benchmark
476 Scientific), and RNA was extracted using Trizol according to the standard protocol (Invitrogen
477 15596018). cDNA synthesis was carried out with a standard oligo-dT primer protocol using the
478 ProtoScript II First Strand cDNA Synthesis Kit (NEB E6560). RNA concentrations were normalized
479 between samples prior to reverse transcription. cDNA was diluted 1:25 in water and used as template
480 for RT-qPCR using the Luna Universal qPCR master mix (NEB M3003S). Primers used are listed in
481 **Supplementary Table 3.** Primer efficiencies were calculated with the formula PCR-efficiency = $10^{(-1/slope)}$

from a linear regression of Cp/ln(DNA) using a serial dilution of each primer with 72 hpf embryo cDNA as described in **Pfaff, 2001**. PCR reactions were performed on a LightCycler 480 II Real Time PCR Instrument (Roche) and analyzed using LightCycler 480 Software. Each RT-qPCR experiment was repeated in triplicate for each biological replicate, and at least two biological replicates were used for each analysis. P-values were calculated using a two-tailed Student's T-test with $\alpha = 0.05$ in Microsoft Excel. Bar charts in **Figure 4** present mean +/- standard error.

**Automated literature screen**

A python script was written to obtain mouse, rat, and human orthologs for a list of zebrafish gene ENSEMBL IDs by obtaining ortholog information relative to each species from BioMart **(Smedley et al. 2009)** and using these downloaded lists as a local database. Once the orthologs were placed in a separate Excel file adjacent to the zebrafish genes, the script obtained GenBank gene names/symbols for all genes and orthologs. Lastly, the script identified the number of PubMed articles containing both the GenBank gene name and keyword input search term by sending GET requests to the NCBI Entrez E-utilities API **(Sayers, 2010)**. In our literature screen, the DEG list of 1,123 genes with FDR adj. $p<0.05$ was used as input with keyword search terms "TGF beta", "Retinoic Acid", "YAP TAZ", and "Piezo". This code has been deposited on GitHub and is publicly available. The URL for the GitHub repository is provided here: **https://github.com/tschilling-lab/Litscreen_Nayak_2022**

**Imaging and *is*HCR quantification**

Whole embryos imaged for ISH were mounted on slides in 80% glycerol and imaged using a Zeiss Axioplan 2 compound microscope utilizing an AxioCam 305 Color Micropublisher 5.0 RTV camera with Zeiss Zen 3.1 (blue edition) software. Embryos imaged for *is*HCR were embedded in 1% low melting point agarose/5x SSC and imaged on a Leica SP8 confocal microscope using the PL APO CS2 40X/1.10 W objective. *is*HCR single cell quantification was performed in ImageJ 1.52p using DAPI as a nuclear

marker. Embryo imaging for a single experiment was performed with identical parameters across conditions. A substack was created from the top and bottom z-slices of each individual cell displaying co-expression of genes of interest, and a maximum intensity Z-projection was created using the substack for each measurement. A ROI of the DAPI-stained nucleus from each Z-projection was traced and pixel-intensity/area was measured. *matn1/scxa* co-expressing cells measured were located at the ch-ih and ch-hh attachment sites, at the posterior edge of the ch cartilage. *klf2a/scxa* and *mxra5b/scxa* co-expressing cells measured were located at the boundaries (myosepta) of somites 16-20. *klf2a/scxa* co-expression was measured primarily in tenocytes near the horizontal myoseptum (HMS) whereas *mxra5b/scxa* co-expression was measured primarily from tenocytes in the ventral half of the vertical myoseptum. All experimental condition data pertaining to each embryo image were kept in a separate document, cell measurements on images were performed, and condition identities were matched to images after measurements. All p-values were calculated using one way ANOVA with $\alpha = 0.05$ and Tukey-Kramer post-hoc tests for pairwise analyses in Microsoft Excel (ns = not significant, * $p < 0.05$, ** $p < 0.01$, *** $p < 0.001$). Box plots in **Figure 4** present median and interquartile range (IQR) with "whiskers" representing largest/smallest value within 1.5*IQR and individual points beyond "whiskers" representing outliers (default R ggplot2 geom_boxplot parameters).

# Acknowledgements:

We thank Danny Dranow for extensive manuscript review, Lianna Fung and David Tatarakis for constructive feedback and helpful discussions; Ines Gehring for fish care; and all other members of the Schilling Lab. Funding sources include NIH grants R01 AR067797, R01 DE013828 and R01 DE030565 to T.F.S.

# Author Contributions:

Conceptualization: A.S., T.S., P.N; Methodology: A.S., T.S., P.N.; Software: P.N.; Validation: P.N., Formal Analysis: P.N.; Investigation: P.N.; Resources: T.S.; Data curation: P.N.; Writing-original draft: P.N., Writing-review and editing: A.S., T.S., P.N.; Visualization: P.N.; Supervision: T.S.; Project administration: P.N.; Funding acquisition: T.S.

# References:

Akutagawa T, Aoki S, Yamamoto-Rikitake M, Iwakiri R, Fujimoto K, Toda S. Cancer-adipose tissue interaction and fluid flow synergistically modulate cell kinetics, HER2 expression, and trastuzumab efficacy in gastric cancer. Gastric Cancer. 2018 Nov;21(6):946-955. doi: 10.1007/s10120-018-0829-7. Epub 2018 Apr 25. PMID: 29696406.

Anderson DM, George R, Noyes MB, Rowton M, Liu W, Jiang R, Wolfe SA, Wilson-Rawls J, Rawls A. Characterization of the DNA-binding properties of the Mohawk homeobox transcription factor. J Biol Chem. 2012 Oct 12;287(42):35351-35359. doi: 10.1074/jbc.M112.399386. Epub 2012 Aug 24. PMID: 22923612; PMCID: PMC3471766.

Balakrishnan L, Nirujogi RS, Ahmad S, Bhattacharjee M, Manda SS, Renuse S, Kelkar DS, Subbannayya Y, Raju R, Goel R, Thomas JK, Kaur N, Dhillon M, Tankala SG, Jois R, Vasdev V, Ramachandra Y, Sahasrabuddhe NA, Prasad TsK, Mohan S, Gowda H, Shankar S, Pandey A. Proteomic analysis of human osteoarthritis synovial fluid. Clin Proteomics. 2014 Feb 17;11(1):6. doi: 10.1186/1559-0275-11-6. PMID: 24533825; PMCID: PMC3942106.

Berthet E, Chen C, Butcher K, Schneider RA, Alliston T, Amirtharajah M. Smad3 binds Scleraxis and Mohawk and regulates tendon matrix organization. J Orthop Res. 2013 Sep;31(9):1475-83. doi: 10.1002/jor.22382. Epub 2013 May 7. PMID: 23653374; PMCID: PMC3960924.

Blitz E, Sharir A, Akiyama H, Zelzer E. Tendon-bone attachment unit is formed modularly by a distinct pool of Scx- and Sox9-positive progenitors. Development. 2013 Jul;140(13):2680-90. doi: 10.1242/dev.093906. Epub 2013 May 29. PMID: 23720048.

Bobzin L, Roberts RR, Chen HJ, Crump JG, Merrill AE. Development and maintenance of tendons and ligaments. Development. 2021 Apr 15;148(8):dev186916. doi: 10.1242/dev.186916. Epub 2021 Apr 16. PMID: 33913478; PMCID: PMC8077520.

Boon RA, Fledderus JO, Volger OL, van Wanrooij EJ, Pardali E, Weesie F, Kuiper J, Pannekoek H, ten Dijke P, Horrevoets AJ. KLF2 suppresses TGF-beta signaling in endothelium through induction of Smad7 and inhibition of AP-1. Arterioscler Thromb Vasc Biol. 2007 Mar;27(3):532-9. doi: 10.1161/01.ATV.0000256466.65450.ce. Epub 2006 Dec 28. PMID: 17194892.

Boselli F, Freund JB, Vermot J. Blood flow mechanics in cardiovascular development. Cell Mol Life Sci. 2015 Jul;72(13):2545-59. doi: 10.1007/s00018-015-1885-3. Epub 2015 Mar 24. PMID: 25801176; PMCID: PMC4457920.

Chen Y, Cossman J, Jayasuriya CT, Li X, Guan Y, Fonseca V, Yang K, Charbonneau C, Yu H, Kanbe K, Ma P, Darling E, Chen Q. Deficient Mechanical Activation of Anabolic Transcripts and Post-Traumatic Cartilage Degeneration in Matrilin-1 Knockout Mice. PLoS One. 2016 Jun 7;11(6):e0156676. doi: 10.1371/journal.pone.0156676. PMID: 27270603; PMCID: PMC4896629.

Chondrogianni N, de C M Simoes D, Franceschi C, Gonos ES. Cloning of differentially expressed genes in skin fibroblasts from centenarians. Biogerontology. 2004;5(6):401-9. doi: 10.1007/s10522-004-3188-1. PMID: 15609104.

568 Chuang HN, Hsiao KM, Chang HY, Wu CC, Pan H. The homeobox transcription factor Irxl1 negatively
569 regulates MyoD expression and myoblast differentiation. FEBS J. 2014 Jul;281(13):2990-3003. doi:
570 10.1111/febs.12837. Epub 2014 May 27. PMID: 24814716.

571 D'Angelo F, Tiribuzi R, Armentano I, Kenny JM, Martino S, Orlacchio A. Mechanotransduction: tuning
572 stem cells fate. J Funct Biomater. 2011 Jun 21;2(2):67-87. doi: 10.3390/jfb2020067. PMID: 24956164;
573 PMCID: PMC4030896.

574 Dobin A, Davis CA, Schlesinger F, Drenkow J, Zaleski C, Jha S, Batut P, Chaisson M, Gingeras TR. STAR:
575 ultrafast universal RNA-seq aligner. Bioinformatics. 2013 Jan 1;29(1):15-21. doi:
576 10.1093/bioinformatics/bts635. Epub 2012 Oct 25. PMID: 23104886; PMCID: PMC3530905.

577 Gabrielsen A, Lawler PR, Yongzhong W, Steinbrüchel D, Blagoja D, Paulsson-Berne G, Kastrup J, Hansson
578 GK. Gene expression signals involved in ischemic injury, extracellular matrix composition and fibrosis
579 defined by global mRNA profiling of the human left ventricular myocardium. J Mol Cell Cardiol. 2007
580 Apr;42(4):870-83. doi: 10.1016/j.yjmcc.2006.12.016. Epub 2007 Jan 8. PMID: 17343875.

581 Hamada H. Role of physical forces in embryonic development. Semin Cell Dev Biol. 2015 Dec;47-48:88-
582 91. doi: 10.1016/j.semcdb.2015.10.011. Epub 2015 Oct 22. PMID: 26474539.

583 He Y, Chen X, Liu H, Xiao H, Kwapong WR, Mei J. Matrix-remodeling associated 5 as a novel tissue
584 biomarker predicts poor prognosis in non-small cell lung cancers. Cancer Biomark. 2015;15(5):645-51.
585 doi: 10.3233/CBM-150504. PMID: 26406953.

586 Ho LTY, Skiba N, Ullmer C, Rao PV. Lysophosphatidic Acid Induces ECM Production via Activation of the
587 Mechanosensitive YAP/TAZ Transcriptional Pathway in Trabecular Meshwork Cells. Invest Ophthalmol
588 Vis Sci. 2018 Apr 1;59(5):1969-1984. doi: 10.1167/iovs.17-23702. PMID: 29677358; PMCID:
589 PMC5896423.

590 Huang da W, Sherman BT, Lempicki RA. Systematic and integrative analysis of large gene lists using
591 DAVID bioinformatics resources. Nat Protoc. 2009;4(1):44-57. doi: 10.1038/nprot.2008.211. PMID:
592 19131956

593 Ireland D, Harrall R, Curry V, Holloway G, Hackney R, Hazleman B, Riley G. Multiple changes in gene
594 expression in chronic human Achilles tendinopathy. Matrix Biol. 2001 Jun;20(3):159-69. doi:
595 10.1016/s0945-053x(01)00128-7. PMID: 11420148.

596 Kaji, D.A., Montero, A.M., Patel, R. et al. Transcriptional profiling of mESC-derived tendon and
597 fibrocartilage cell fate switch. Nat Commun 12, 4208 (2021). https://doi.org/10.1038/s41467-021-
598 24535-5

599 Kang JS, Alliston T, Delston R, Derynck R. Repression of Runx2 function by TGF-beta through recruitment
600 of class II histone deacetylases by Smad3. EMBO J. 2005 Jul 20;24(14):2543-55. doi:
601 10.1038/sj.emboj.7600729. Epub 2005 Jun 30. PMID: 15990875; PMCID: PMC1176457.

602 Keller R, Shook D, Skoglund P. The forces that shape embryos: physical aspects of convergent extension
603 by cell intercalation. Phys Biol. 2008 Apr 10;5(1):015007. doi: 10.1088/1478-3975/5/1/015007. PMID:
604 18403829. Kimmel CB, Ballard WW,

605 Kimmel SR, Ullmann B, Schilling TF. Stages of embryonic development of the zebrafish. Dev Dyn. 1995
606 Jul;203(3):253-310. doi: 10.1002/aja.1002030302. PMID: 8589427.

607 Kult S, Olender T, Osterwalder M, Markman S, Leshkowitz D, Krief S, Blecher-Gonen R, Ben-Moshe S,
608 Farack L, Keren-Shaul H, Salame TM, Capellini TD, Itzkovitz S, Amit I, Visel A, Zelzer E. Bi-fated tendon-to-
609 bone attachment cells are regulated by shared enhancers and KLF transcription factors. Elife. 2021 Jan
610 15;10:e55361. doi: 10.7554/eLife.55361. PMID: 33448926; PMCID: PMC7810463.

611 Laue K, Jänicke M, Plaster N, Sonntag C, Hammerschmidt M. Restriction of retinoic acid activity by
612 Cyp26b1 is required for proper timing and patterning of osteogenesis during zebrafish development.
613 Development. 2008 Nov;135(22):3775-87. doi: 10.1242/dev.021238. Epub 2008 Oct 16. PMID:
614 18927157; PMCID: PMC3608526.

615 Lee JS, Yu Q, Shin JT, Sebzda E, Bertozzi C, Chen M, Mericko P, Stadtfeld M, Zhou D, Cheng L, Graf T,
616 MacRae CA, Lepore JJ, Lo CW, Kahn ML. Klf2 is an essential regulator of vascular hemodynamic forces in
617 vivo. Dev Cell. 2006 Dec;11(6):845-57. doi: 10.1016/j.devcel.2006.09.006. PMID: 17141159.

618 Lee W, Nims RJ, Savadipour A, Zhang Q, Leddy HA, Liu F, McNulty AL, Chen Y, Guilak F, Liedtke WB.
619 Inflammatory signaling sensitizes Piezo1 mechanotransduction in articular chondrocytes as a pathogenic
620 feed-forward mechanism in osteoarthritis. Proc Natl Acad Sci U S A. 2021 Mar 30;118(13):e2001611118.
621 doi: 10.1073/pnas.2001611118. PMID: 33758095; PMCID: PMC8020656.

622 Li B, Dewey CN. RSEM: accurate transcript quantification from RNA-Seq data with or without a reference
623 genome. BMC Bioinformatics. 2011 Aug 4;12:323. doi: 10.1186/1471-2105-12-323. PMID: 21816040;
624 PMCID: PMC3163565.

625 Li H, Wang Y, Liu J, Chen X, Duan Y, Wang X, Shen Y, Kuang Y, Zhuang T, Tomlinson B, Chan P, Yu Z, Cheng
626 Y, Zhang L, Liu Z, Zhang Y, Zhao Z, Zhang Q, Liu J. Endothelial Klf2-Foxp1-TGFβ signal mediates the
627 inhibitory effects of simvastatin on maladaptive cardiac remodeling. Theranostics. 2021 Jan
628 1;11(4):1609-1625. doi: 10.7150/thno.48153. PMID: 33408770; PMCID: PMC7778601.

629 Liu D, Black BL, Derynck R. TGF-beta inhibits muscle differentiation through functional repression of
630 myogenic transcription factors by Smad3. Genes Dev. 2001 Nov 15;15(22):2950-66. doi:
631 10.1101/gad.925901. PMID: 11711431; PMCID: PMC312830.

632 Lorda-Diez CI, Montero JA, Diaz-Mendoza MJ, Garcia-Porrero JA, Hurle JM. Defining the earliest
633 transcriptional steps of chondrogenic progenitor specification during the formation of the digits in the
634 embryonic limb. PLoS One. 2011;6(9):e24546. doi: 10.1371/journal.pone.0024546. Epub 2011 Sep 13.
635 PMID: 21931747; PMCID: PMC3172225.

636 Lou W, Liu J, Ding B, Jin L, Xu L, Li X, Chen J, Fan W. Five miRNAs-mediated PIEZO2 downregulation,
637 accompanied with activation of Hedgehog signaling pathway, predicts poor prognosis of breast cancer.
638 Aging (Albany NY). 2019 May 6;11(9):2628-2652. doi: 10.18632/aging.101934. PMID: 31058608; PMCID:
639 PMC6535055.

640 Lu HH, Thomopoulos S. Functional attachment of soft tissues to bone: development, healing, and tissue
641 engineering. Annu Rev Biomed Eng. 2013;15:201-26. doi: 10.1146/annurev-bioeng-071910-124656.
642 Epub 2013 Apr 29. Erratum in: Annu Rev Biomed Eng. 2013;15:vi. PMID: 23642244; PMCID:
643 PMC3925419.

644 Maeda T, Sakabe T, Sunaga A, Sakai K, Rivera AL, Keene DR, Sasaki T, Stavnezer E, Iannotti J, Schweitzer
645 R, Ilic D, Baskaran H, Sakai T. Conversion of mechanical force into TGF-β-mediated biochemical signals.

Curr Biol. 2011 Jun 7;21(11):933-41. doi: 10.1016/j.cub.2011.04.007. Epub 2011 May 19. PMID: 21600772; PMCID: PMC3118584.

McGurk PD, Swartz ME, Chen JW, Galloway JL, Eberhart JK. In vivo zebrafish morphogenesis shows Cyp26b1 promotes tendon condensation and musculoskeletal patterning in the embryonic jaw. PLoS Genet. 2017 Dec 11;13(12):e1007112. doi: 10.1371/journal.pgen.1007112. PMID: 29227993; PMCID: PMC5739505.

McNeilly CM, Banes AJ, Benjamin M, Ralphs JR. Tendon cells in vivo form a three dimensional network of cell processes linked by gap junctions. J Anat. 1996 Dec;189 ( Pt 3)(Pt 3):593-600. Erratum in: J Anat 1997 Apr;190(Pt 3):477-8. PMID: 8982835; PMCID: PMC1167702.

Memon A, Lee WK. KLF10 as a Tumor Suppressor Gene and Its TGF-β Signaling. Cancers (Basel). 2018 May 25;10(6):161. doi: 10.3390/cancers10060161. PMID: 29799499; PMCID: PMC6025274.

Metsalu T, Vilo J. ClustVis: a web tool for visualizing clustering of multivariate data using Principal Component Analysis and heatmap. Nucleic Acids Res. 2015 Jul 1;43(W1):W566-70. doi: 10.1093/nar/gkv468. Epub 2015 May 12. PMID: 25969447; PMCID: PMC4489295.

Mi H, Thomas P. PANTHER pathway: an ontology-based pathway database coupled with data analysis tools. Methods Mol Biol. 2009;563:123-40. doi: 10.1007/978-1-60761-175-2_7. PMID: 19597783; PMCID: PMC6608593

Pei M, Luo J, Chen Q. Enhancing and maintaining chondrogenesis of synovial fibroblasts by cartilage extracellular matrix protein matrilins. Osteoarthritis Cartilage. 2008 Sep;16(9):1110-7. doi: 10.1016/j.joca.2007.12.011. Epub 2008 Feb 20. PMID: 18282772; PMCID: PMC2596998.

Pfaffl MW. A new mathematical model for relative quantification in real-time RT-PCR. Nucleic Acids Res. 2001 May 1;29(9):e45. doi: 10.1093/nar/29.9.e45. PMID: 11328886; PMCID: PMC55695.

Picelli S, Faridani OR, Björklund AK, Winberg G, Sagasser S, Sandberg R. Full-length RNA-seq from single cells using Smart-seq2. Nat Protoc. 2014 Jan;9(1):171-81. doi: 10.1038/nprot.2014.006. Epub 2014 Jan 2. PubMed PMID: 24385147.

Pingel J, Lu Y, Starborg T, Fredberg U, Langberg H, Nedergaard A, Weis M, Eyre D, Kjaer M, Kadler KE. 3-D ultrastructure and collagen composition of healthy and overloaded human tendon: evidence of tenocyte and matrix buckling. J Anat. 2014 May;224(5):548-55. doi: 10.1111/joa.12164. Epub 2014 Feb 9. PMID: 24571576; PMCID: PMC3981497.

Poveda J, Sanz AB, Fernandez-Fernandez B, Carrasco S, Ruiz-Ortega M, Cannata-Ortiz P, Ortiz A, Sanchez-Niño MD. MXRA5 is a TGF-β1-regulated human protein with anti-inflammatory and anti-fibrotic properties. J Cell Mol Med. 2017 Jan;21(1):154-164. doi: 10.1111/jcmm.12953. Epub 2016 Sep 6. PMID: 27599751; PMCID: PMC5192817.

Pryce BA, Watson SS, Murchison ND, Staverosky JA, Dünker N, Schweitzer R. Recruitment and maintenance of tendon progenitors by TGFbeta signaling are essential for tendon formation. Development. 2009 Apr;136(8):1351-61. doi: 10.1242/dev.027342. PMID: 19304887; PMCID: PMC2687466.

Riley SE, Feng Y, Hansen CG. Hippo-Yap/Taz signalling in zebrafish regeneration. NPJ Regen Med. 2022 Jan 27;7(1):9. doi: 10.1038/s41536-022-00209-8. PMID: 35087046; PMCID: PMC8795407.

685 Robins JE, Capehart AA. Matrix remodeling associated 5 expression in trunk and limb during avian
686 development. Int J Dev Biol. 2018;62(4-5):335-340. doi: 10.1387/ijdb.170225ac. PMID: 29877573.

687 Rullman E, Norrbom J, Strömberg A, Wågsäter D, Rundqvist H, Haas T, Gustafsson T. Endurance exercise
688 activates matrix metalloproteinases in human skeletal muscle. J Appl Physiol (1985). 2009
689 Mar;106(3):804-12. doi: 10.1152/japplphysiol.90872.2008. Epub 2009 Jan 8. PMID: 19131480.

690 Sayers E. A General Introduction to the E-utilities. In: Entrez Programming Utilities Help [Internet].
691 Bethesda (MD): National Center for Biotechnology Information (US); 2010-. Available from:
692 https://www.ncbi.nlm.nih.gov/books/NBK25497/

693 Schilling TF, Kimmel CB. Musculoskeletal patterning in the pharyngeal segments of the zebrafish
694 embryo. Development. 1997 Aug;124(15):2945-60. doi: 10.1242/dev.124.15.2945. PMID: 9247337.

695 Schweitzer R, Zelzer E, Volk T. Connecting muscles to tendons: tendons and musculoskeletal
696 development in flies and vertebrates. Development. 2010 Sep 1;137(17):2807-17. doi:
697 10.1242/dev.047498. Erratum in: Development. 2010 Oct;137(19):3347. PMID: 20699295; PMCID:
698 PMC2938915.

699 Smedley D, Haider S, Ballester B, Holland R, London D, Thorisson G, Kasprzyk A. BioMart--biological
700 queries made easy. BMC Genomics. 2009 Jan 14;10:22. doi: 10.1186/1471-2164-10-22. PMID:
701 19144180; PMCID: PMC2649164.

702 Steed E, Faggianelli N, Roth S, Ramspacher C, Concordet JP, Vermot J. klf2a couples
703 mechanotransduction and zebrafish valve morphogenesis through fibronectin synthesis. Nat Commun.
704 2016 May 25;7:11646. doi: 10.1038/ncomms11646. PubMed PMID: 27221222; PubMed Central PMCID:
705 PMC4894956.

706 Subramanian A, Kanzaki LF, Galloway JL, Schilling TF. Mechanical force regulates tendon extracellular
707 matrix organization and tenocyte morphogenesis through TGFbeta signaling. Elife. 2018 Nov 26;7. pii:
708 e38069. doi: 10.7554/eLife.38069. PubMed PMID: 30475205; PubMed Central PMCID: PMC6345564.

709 Subramanian A, Schilling TF. Tendon development and musculoskeletal assembly: emerging roles for the
710 extracellular matrix. Development. 2015 Dec 15;142(24):4191-204. doi: 10.1242/dev.114777. PMID:
711 26672092; PMCID: PMC4689213.

712 Subramanian A, Schilling TF. Thrombospondin-4 controls matrix assembly during development and
713 repair of myotendinous junctions. Elife. 2014 Jun 18;3:e02372. doi: 10.7554/eLife.02372. PMID:
714 24941943; PMCID: PMC4096842.

715 Swinburne IA, Mosaliganti KR, Green AA, Megason SG. Improved Long-Term Imaging of Embryos with
716 Genetically Encoded α-Bungarotoxin. PLoS One. 2015 Aug 5;10(8):e0134005. doi:
717 10.1371/journal.pone.0134005. PMID: 26244658; PMCID: PMC4526548.

718 Thisse C, Thisse B, Schilling TF, Postlethwait JH. Structure of the zebrafish snail1 gene and its expression
719 in wild-type, spadetail and no tail mutant embryos. Development. 1993 Dec;119(4):1203-15. doi:
720 10.1242/dev.119.4.1203. PMID: 8306883.

721 Wang GH, Yao L, Xu HW, Tang WT, Fu JH, Hu XF, Cui L, Xu XM. Identification of MXRA5 as a novel
722 biomarker in colorectal cancer. Oncol Lett. 2013 Feb;5(2):544-548. doi: 10.3892/ol.2012.1038. Epub
723 2012 Nov 21. PMID: 23420087; PMCID: PMC3573052.

724 Wang JH. Mechanobiology of tendon. J Biomech. 2006;39(9):1563-82. doi:
725 10.1016/j.jbiomech.2005.05.011. Epub 2005 Jul 5. PMID: 16000201.

726 Westerfield M (2007) The Zebrafish Book: A Guide for the Laboratory Use of Zebrafish (Danio Rerio (Fifth
727 edition) Eugene, Oregon: University of Oregon Press.

728 Wu T, Hu E, Xu S, Chen M, Guo P, Dai Z, Feng T, Zhou L, Tang W, Zhan L, Fu X, Liu S, Bo X, Yu G.
729 clusterProfiler 4.0: A universal enrichment tool for interpreting omics data. Innovation (N Y). 2021 Jul
730 1;2(3):100141. doi: 10.1016/j.xinn.2021.100141. PMID: 34557778; PMCID: PMC8454663.

731 Zelzer E, Blitz E, Killian ML, Thomopoulos S. Tendon-to-bone attachment: from development to maturity.
732 Birth Defects Res C Embryo Today. 2014 Mar;102(1):101-12. doi: 10.1002/bdrc.21056. PMID: 24677726;
733 PMCID: PMC4076491.

734 Zhang M, Meng N, Wang X, Chen W, Zhang Q. TRPV4 and PIEZO Channels Mediate the Mechanosensing
735 of Chondrocytes to the Biomechanical Microenvironment. Membranes (Basel). 2022 Feb 18;12(2):237.
736 doi: 10.3390/membranes12020237. PMID: 35207158; PMCID: PMC8874592.

737 Zhou W, Saint-Amant L, Hirata H, Cui WW, Sprague SM, Kuwada JY. Non-sense mutations in the
738 dihydropyridine receptor beta1 gene, CACNB1, paralyze zebrafish relaxed mutants. Cell Calcium. 2006
739 Mar;39(3):227-36. doi: 10.1016/j.ceca.2005.10.015. Epub 2005 Dec 20. PMID: 16368137.

# Figure 1

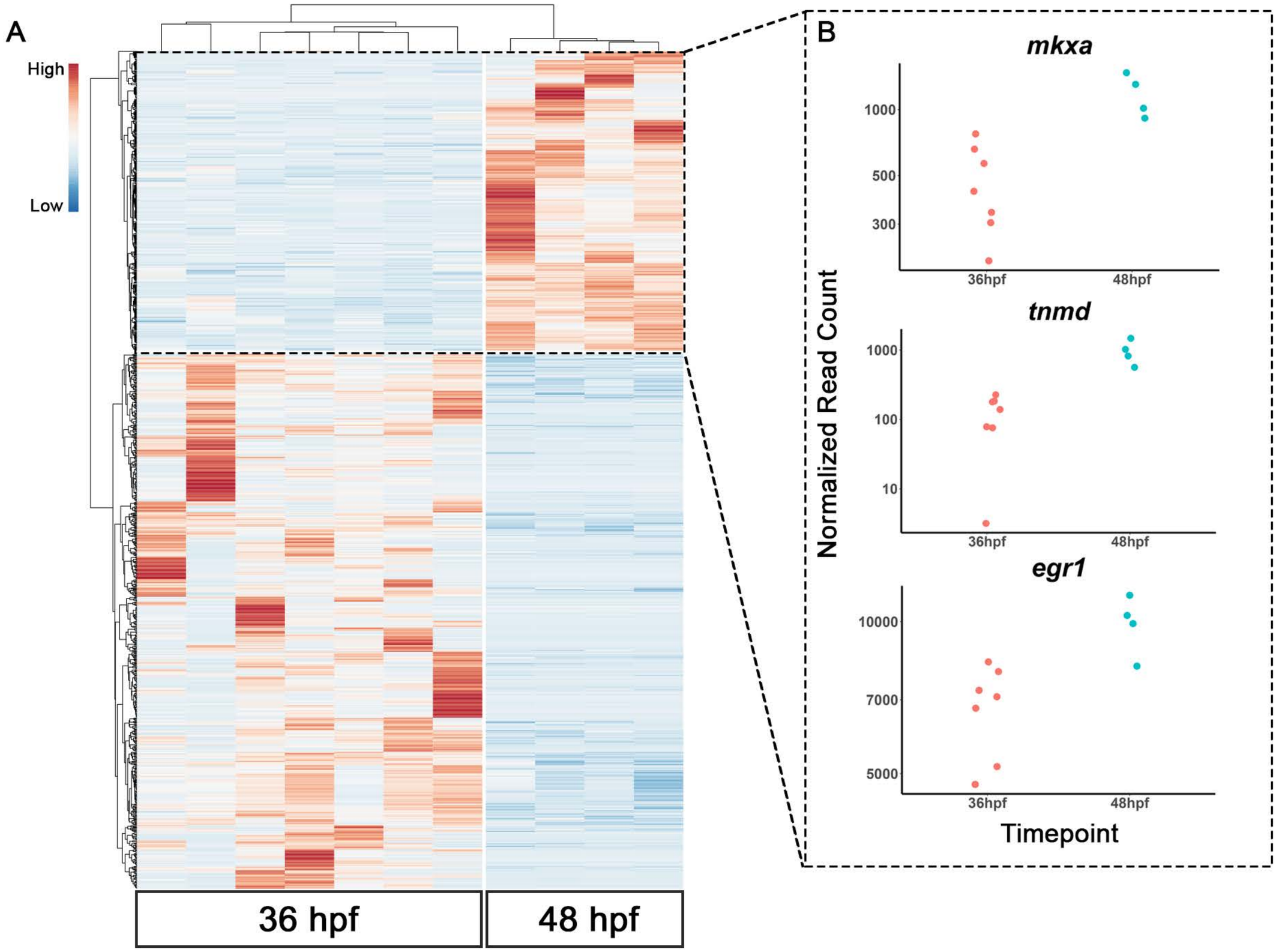


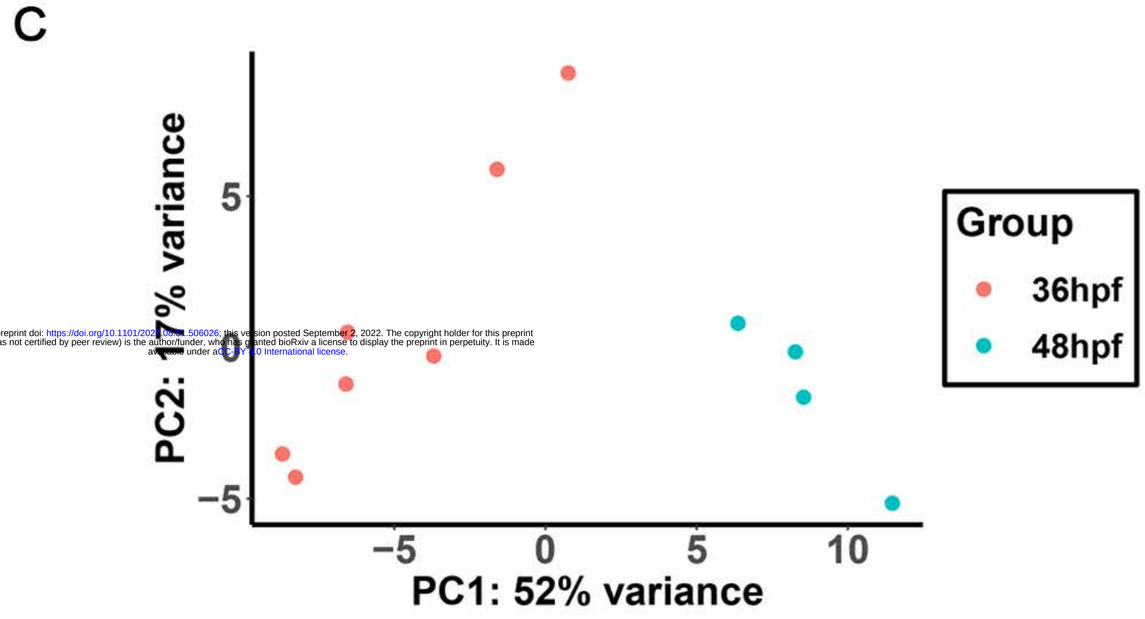


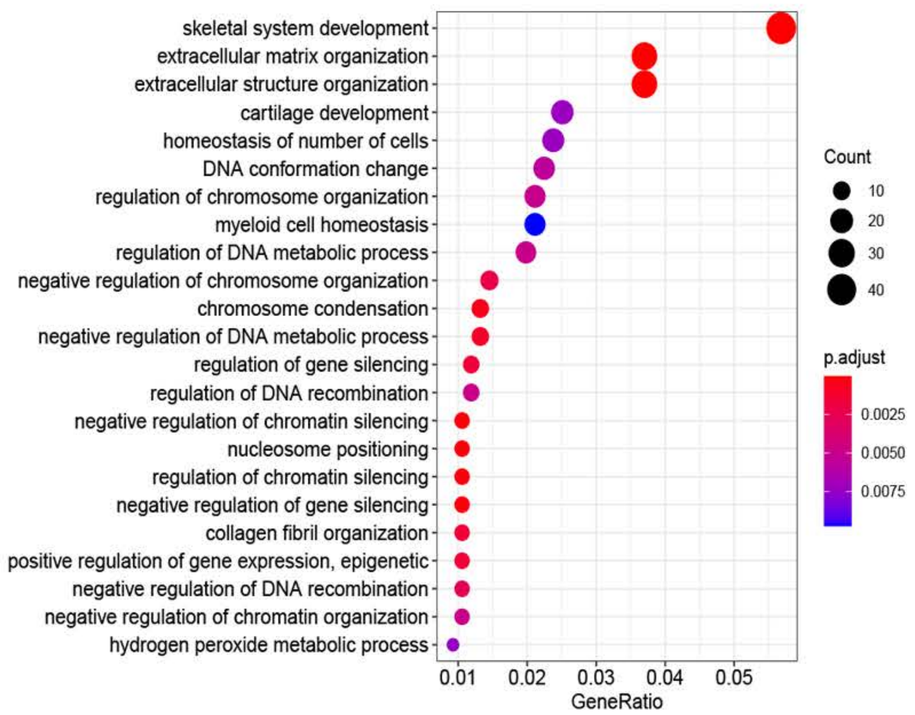

Figure 2

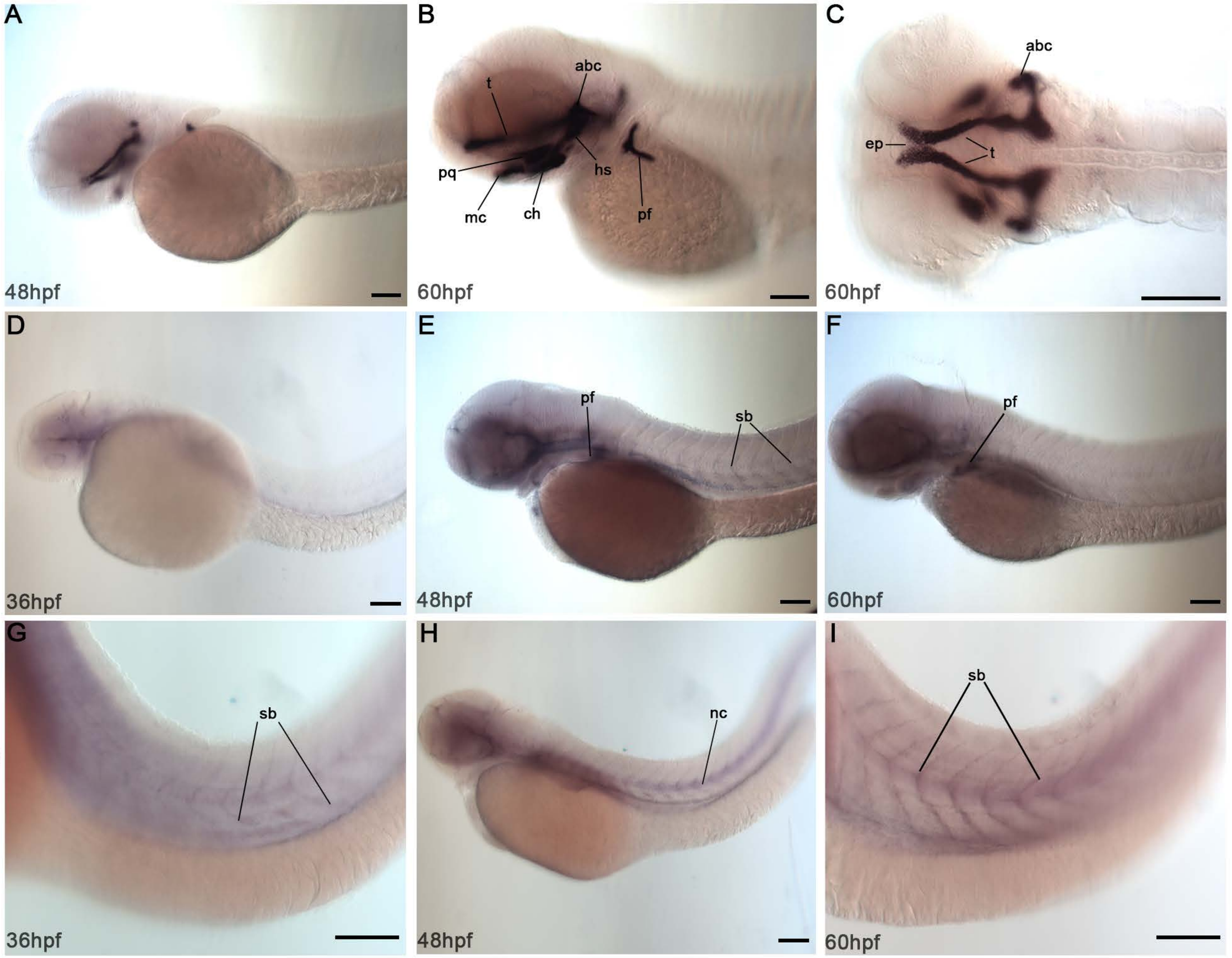

# Figure 3

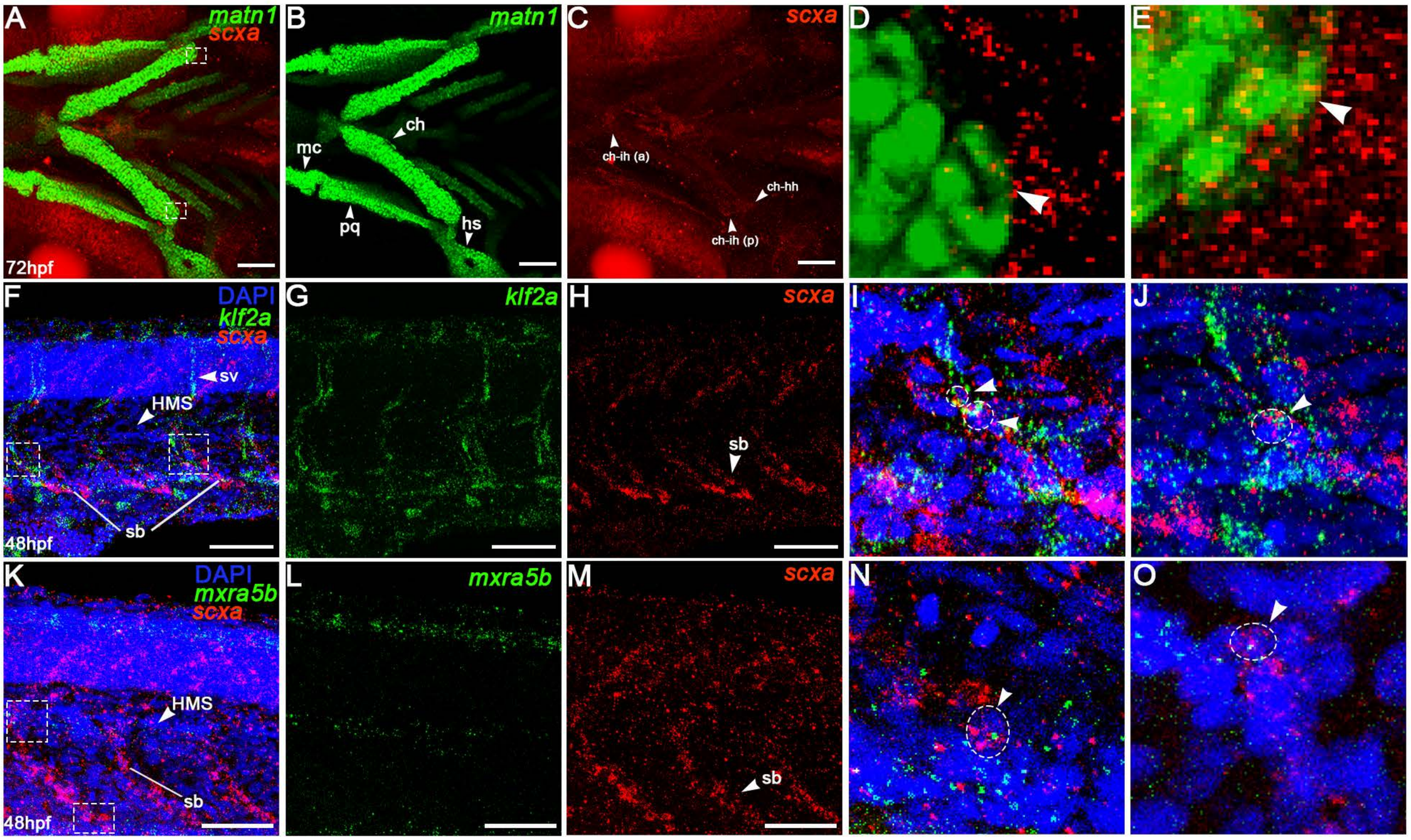

Figure 4

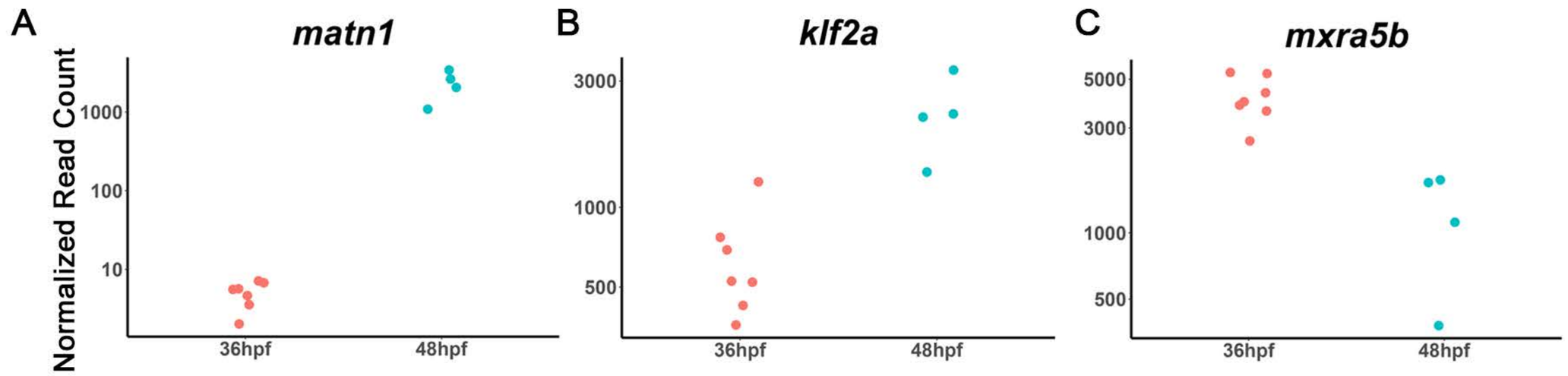


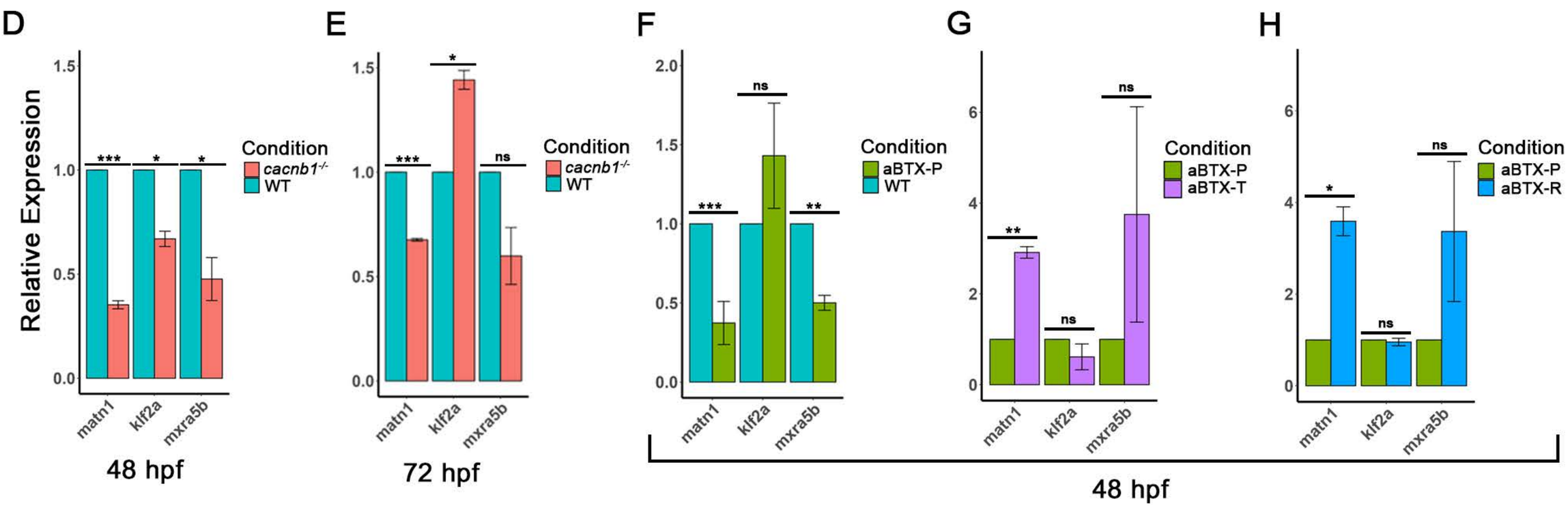


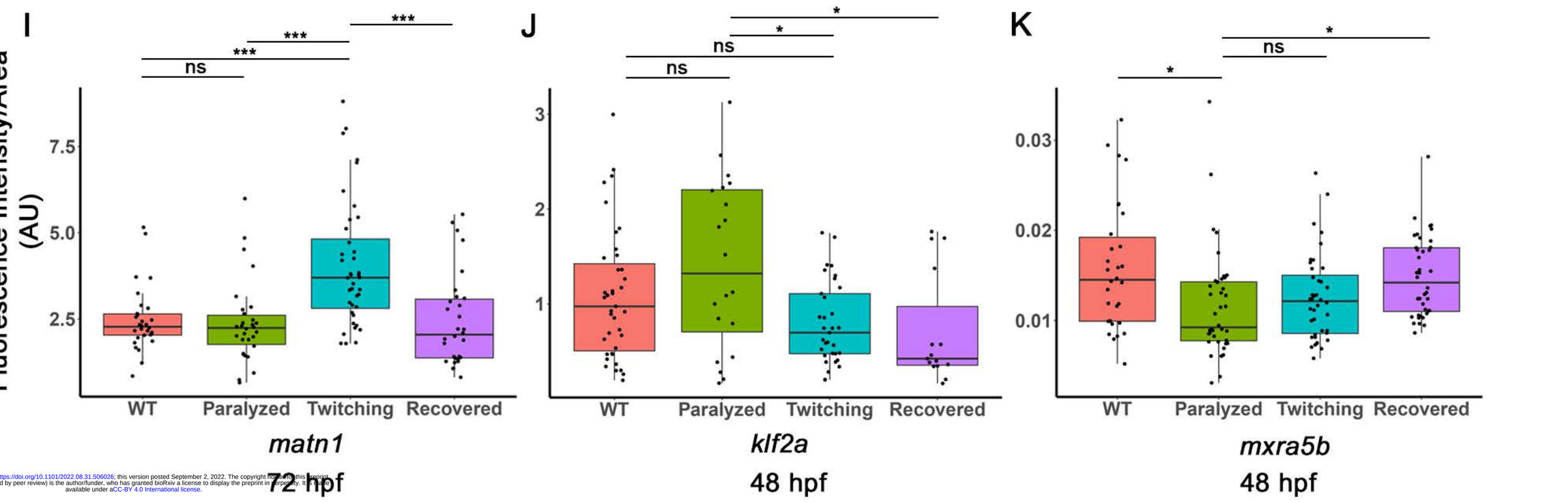

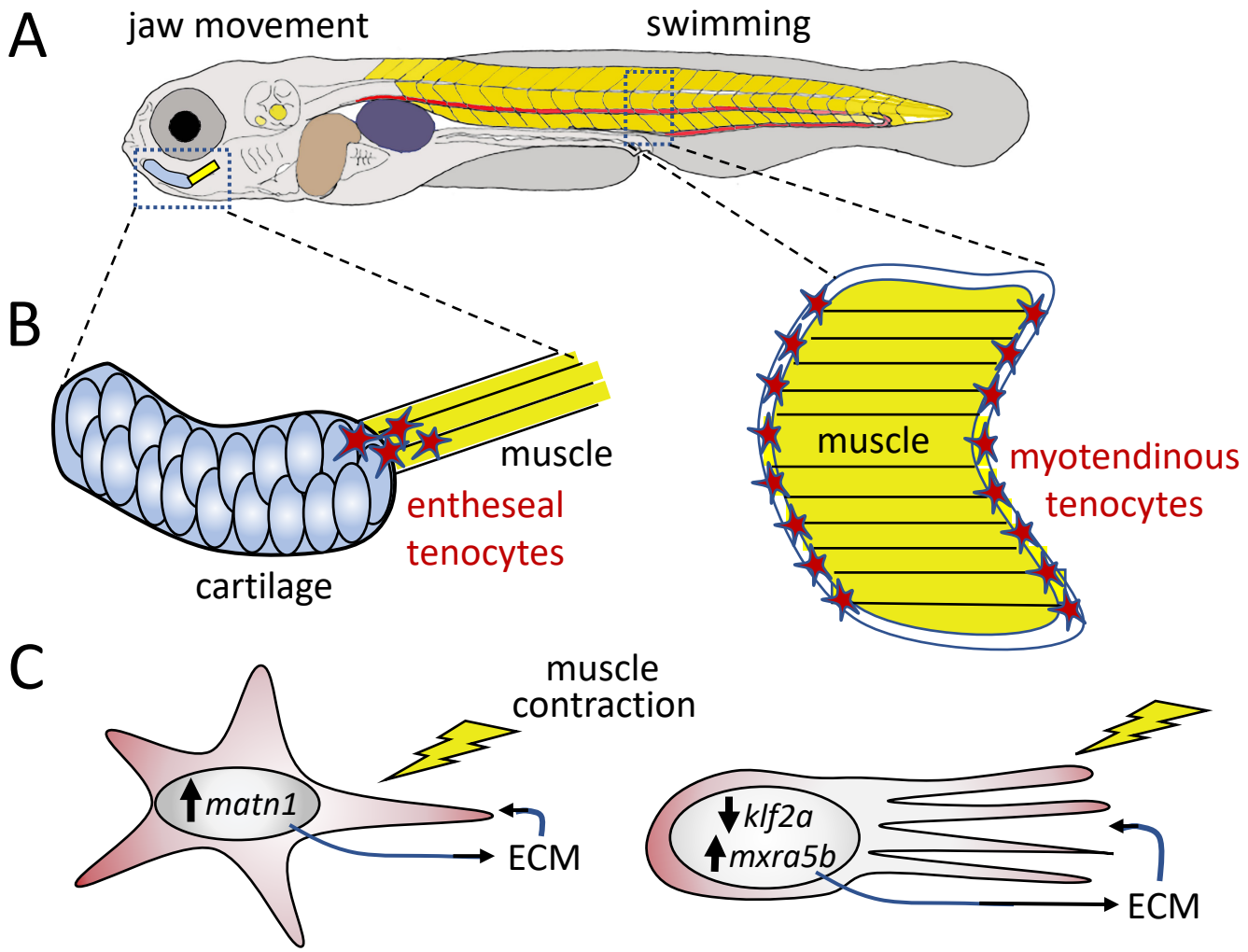
A
jaw movement
swimming
B
muscle
entheseal
tenocytes
cartilage
muscle
myotendinous
tenocytes
C
muscle
contraction
matn1
ECM
klf2a
mxra5b
ECM

# Supplementary Figure 1

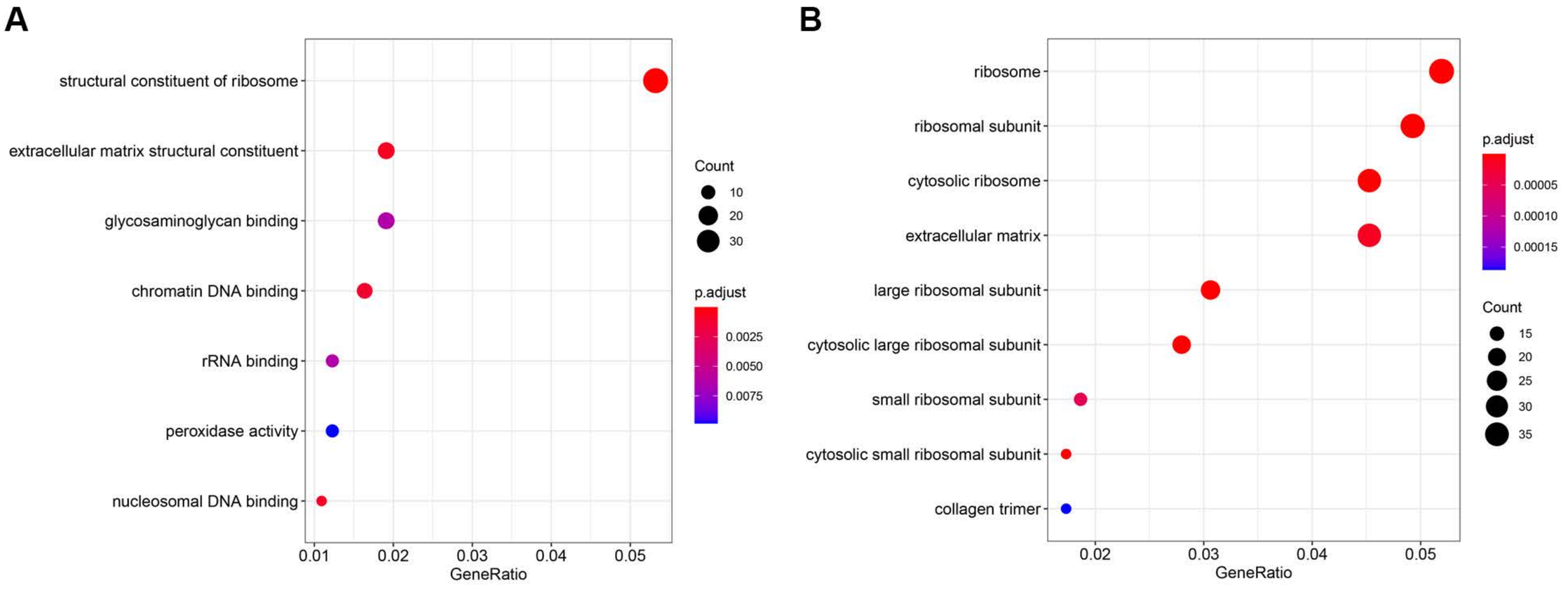

# Supplementary Figure 2

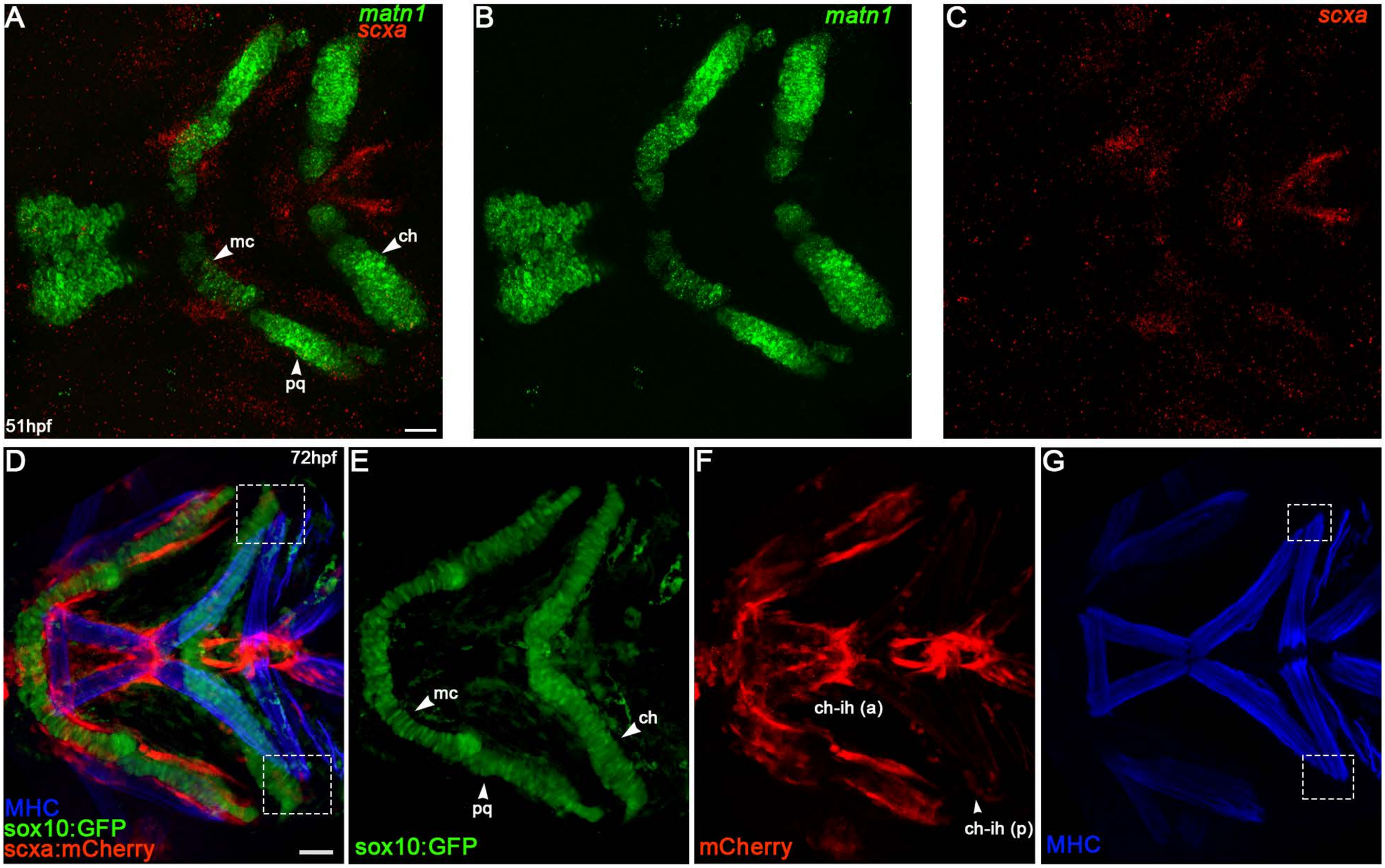

## Supplementary Table 1

**PANTHER Bioinformatics Pathway Analysis**

| PANTHER Pathway | Number of Genes | Genes | | | | | | | | | | | | | | | | |
|---|---|---|---|---|---|---|---|---|---|---|---|---|---|---|---|---|---|---|
| Gonadotropin-releasing hormone receptor pathway (P06664) | 17 | *prkag1* | *prkcg* | *atf2* | *egr1* | *fsta* | *tgfb3* | *fosb* | *fstb* | *jun* | *tuba1c* | *jund* | *junbb* | *atf3* | *fosab* | *id3* | *cacna1sa* | *nfatc1* |
| CCKR signaling map (P06959) | 16 | *nfkbiab* | *prkcg* | *atf2* | *egr1* | *mycb* | *hbegfa* | *foxo3b* | *gcgb* | *mcl1a* | *nfkbiaa* | *tacr1a* | *mcl1b* | *jun* | *mych* | *fosab* | *bcar1* | |
| Wnt signaling pathway (P00057) | 16 | *fzd3b* | *csnk1da* | *prkcg* | *mycb* | *cdh18a* | ppp2r5a | smarcd3a | cdh11 | wnt7aa | celsr1b | fzd7a | wnt11 | actc1b | mych | tbxtb | nfatc1 | |
| Apoptosis signaling pathway (P00006) | 13 | jdp2 | nfkbiab | prkcq | atf2 | mcl1a | nfkbiaa | atf4b | fosb | mcl1b | jun | atf3 | bcl2l10 | fosab | | | | |
| Integrin signalling pathway (P00034) | 13 | col1a1a | col11a2 | col18a1a | col9a3 | itgb6 | col5a2b | col8a1a | actn3b | col6a1 | actn3a | bcar1 | col11a1a | si:ch211-195o20.7 | | | | |
| Inflammation mediated by chemokine and cytokine signaling pathway (P00031) | 12 | nfkbiab | nfkbiaa | plcd4b | jun | actc1b | jund | junbb | myh9a | myh9b | col6a1 | grap2a | nfatc1 | | | | | |
| TGF-beta signaling pathway (P00052) | 10 | atf2 | smurf2 | bmp8a | tgfb3 | acvrl1 | jun | jund | gdf6b | junbb | gdf5 | | | | | | | |
| PDGF signaling pathway (P00047) | 10 | arhgap27l | gab1 | nin | mycb | fosb | jun | mapk15 | mych | fosab | grap2a | | | | | | | |
| Angiogenesis (P00005) | 9 | hif1ab | fzd3b | prkcq | pld2 | wnt7aa | fosb | f3b | jun | fosab | | | | | | | | |
| Huntington disease (P00029) | 9 | dynll2b | tp73 | capn3b | si:ch211-251b21.1 | fosb | jun | actc1b | fosab | tubb6 | | | | | | | | |
| Cadherin signaling pathway (P00012) | 8 | fzd3b | cdh18a | cdh11 | wnt7aa | celsr1b | fzd7a | wnt11 | actc1b | | | | | | | | | |
| Alzheimer disease-presenilin pathway (P00004) | 7 | fzd3b | wnt7aa | fzd7a | furina | wnt11 | actc1b | appb | | | | | | | | | | |
| T cell activation (P00053) | 7 | nfkbiab | prkcq | nfkbiaa | jun | fosab | grap2a | nfatc1 | | | | | | | | | | |
| Cytoskeletal regulation by Rho GTPase (P00016) | 7 | si:ch211-203d1.3 | actc1b | ssh2b | rock2a | myh9a | myh9b | tubb6 | | | | | | | | | | |
| Parkinson disease (P00049) | 6 | sncb | csnk1da | pld2 | mapk15 | uchl1 | hck | | | | | | | | | | | |
| Oxidative stress response (P00046) | 6 | atf2 | mycb | dusp8a | jun | dusp2 | mych | | | | | | | | | | | |
| Nicotinic acetylcholine receptor signaling pathway (P00044) | 6 | myo1f | vamp2 | actc1b | myh9a | myh9b | cacna1sa | | | | | | | | | | | |
| Interleukin signaling pathway (P00036) | 6 | mycb | foxo3b | mapk15 | il16 | mych | fosab | | | | | | | | | | | |
| Oxytocin receptor mediated signaling pathway (P04391) | 6 | prkcq | gnb3a | gngt2a | vamp2 | plcd4b | cacna1sa | | | | | | | | | | | |
| Heterotrimeric G-protein signaling pathway-Gi alpha and Gs alpha mediated pathway (P00026) | 6 | rgs7b | gngt2a | si:ch211-272n13.7 | grk1a | adrb3a | adra1d | | | | | | | | | | | |
| 5HT2 type receptor mediated signaling pathway (P04374) | 6 | prkcq | gnb3a | gngt2a | vamp2 | plcd4b | cacna1sa | | | | | | | | | | | |
| Alzheimer disease-amyloid secretase pathway (P00003) | 5 | prkcq | furina | mapk15 | appb | cacna1sa | | | | | | | | | | | | |
| Muscarinic acetylcholine receptor 1 and 3 signaling pathway (P00042) | 5 | prkcq | gnb3a | gngt2a | vamp2 | kcnq2b | | | | | | | | | | | | |
| Metabotropic glutamate receptor group II pathway (P00040) | 5 | gnb3a | gngt2a | vamp2 | si:ch211-272n13.7 | gnao1b | | | | | | | | | | | | |
| Metabotropic glutamate receptor group III pathway (P00039) | 5 | gnb3a | gngt2a | vamp2 | si:ch211-251b21.1 | si:ch211-272n13.7 | | | | | | | | | | | | |
| Thyrotropin-releasing hormone receptor signaling pathway (P04394) | 5 | prkcq | gnb3a | gngt2a | vamp2 | plcd4b | | | | | | | | | | | | |
| EGF receptor signaling pathway (P00018) | 5 | gab1 | prkcq | hbegfa | ppp2r5a | mapk15 | | | | | | | | | | | | |
| Beta2 adrenergic receptor signaling pathway (P04378) | 5 | gnb3a | gngt2a | vamp2 | si:ch211-272n13.7 | cacna1sa | | | | | | | | | | | | |
| B cell activation (P00010) | 5 | nfkbiab | nfkbiaa | jun | fosab | nfatc1 | | | | | | | | | | | | |
| Beta1 adrenergic receptor signaling pathway (P04377) | 5 | gnb3a | gngt2a | vamp2 | si:ch211-272n13.7 | cacna1sa | | | | | | | | | | | | |
| Ubiquitin proteasome pathway (P00060) | 4 | smurf2 | huwe1 | nedd4a | ube2a | | | | | | | | | | | | | |
| Toll receptor signaling pathway (P00054) | 4 | nfkbiab | nfkbiaa | jun | tlr4ba | | | | | | | | | | | | | |
| Muscarinic acetylcholine receptor 2 and 4 signaling pathway (P00043) | 4 | gnb3a | gngt2a | vamp2 | si:ch211-272n13.7 | | | | | | | | | | | | | |
| Insulin/IGF pathway-mitogen activated protein kinase kinase/MAP kinase cascade (P00032) | 4 | igf2a | igf2b | fosb | fosab | | | | | | | | | | | | | |
| Opioid proopiomelanocortin pathway (P05917) | 4 | gnb3a | gngt2a | vamp2 | gnao1b | | | | | | | | | | | | | |
| Opioid prodynorphin pathway (P05916) | 4 | gnb3a | gngt2a | vamp2 | gnao1b | | | | | | | | | | | | | |
| Enkephalin release (P05913) | 4 | gnb3a | gngt2a | si:ch211-272n13.7 | gnao1b | | | | | | | | | | | | | |
| FGF signaling pathway (P00021) | 4 | fgf10a | prkcq | ppp2r5a | fgf10b | | | | | | | | | | | | | |
| Histamine H1 receptor mediated signaling pathway (P04385) | 4 | prkcq | gnb3a | gngt2a | plcd4b | | | | | | | | | | | | | |
| Endothelin signaling pathway (P00019) | 4 | prkcq | ednrab | furina | si:ch211-272n13.7 | | | | | | | | | | | | | |
| Beta3 adrenergic receptor signaling pathway (P04379) | 4 | gnb3a | gngt2a | vamp2 | adrb3a | | | | | | | | | | | | | |
| 5HT1 type receptor mediated signaling pathway (P04373) | 4 | gnb3a | gngt2a | vamp2 | si:ch211-272n13.7 | | | | | | | | | | | | | |
| Notch signaling pathway (P00045) | 3 | hey1 | neurl4 | neurl1aa | | | | | | | | | | | | | | |
| Ionotropic glutamate receptor pathway (P00037) | 3 | vamp2 | si:ch211-251b21.1 | pick1 | | | | | | | | | | | | | | |
| Insulin/IGF pathway-protein kinase B signaling cascade (P00033) | 3 | igf2a | igf2b | foxo3b | | | | | | | | | | | | | | |
| p53 pathway feedback loops 2 (P04398) | 3 | tp73 | mycb | mych | | | | | | | | | | | | | | |
| Ras Pathway (P04393) | 3 | atf2 | pld2 | jun | | | | | | | | | | | | | | |
| Heterotrimeric G-protein signaling pathway-rod outer segment phototransduction (P00028) | 3 | gngt2a | cngb1b | grk1a | | | | | | | | | | | | | | |
| Heterotrimeric G-protein signaling pathway-Gq alpha and Go alpha mediated pathway (P00027) | 3 | prkcq | rgs7b | gngt2a | | | | | | | | | | | | | | |
| Hedgehog signaling pathway (P00025) | 3 | csnk1da | si:ch211-272n13.7 | gli2b | | | | | | | | | | | | | | |
| Opioid proenkephalin pathway (P05915) | 3 | gnb3a | gngt2a | vamp2 | | | | | | | | | | | | | | |
| Dopamine receptor mediated signaling pathway (P05912) | 3 | vamp2 | si:ch211-272n13.7 | ppp1caa | | | | | | | | | | | | | | |
| Histamine H2 receptor mediated signaling pathway (P04386) | 3 | gnb3a | gngt2a | si:ch211-272n13.7 | | | | | | | | | | | | | | |
| Cortocotropin releasing factor receptor signaling pathway (P04380) | 3 | gnb3a | gngt2a | vamp2 | | | | | | | | | | | | | | |
| DNA replication (P00017) | 3 | top2a | h3f3d | pcna | | | | | | | | | | | | | | |
| Blood coagulation (P00011) | 3 | f10 | f3b | appb | | | | | | | | | | | | | | |
| 5HT4 type receptor mediated signaling pathway (P04376) | 3 | gnb3a | gngt2a | vamp2 | | | | | | | | | | | | | | |
| Toll pathway-drosophila (P06217) | 2 | nfkbiab | nfkbiaa | | | | | | | | | | | | | | | |
| Axon guidance mediated by Slit/Robo (P00008) | 2 | slit1a | obscnb | | | | | | | | | | | | | | | |
| Alpha adrenergic receptor signaling pathway (P00002) | 2 | vamp2 | adra1d | | | | | | | | | | | | | | | |
| p53 pathway (P00059) | 2 | tp73 | rrm2 | | | | | | | | | | | | | | | |
| VEGF signaling pathway (P00056) | 2 | hif1ab | prkcq | | | | | | | | | | | | | | | |
| Transcription regulation by bZIP transcription factor (P00055) | 2 | si:ch211-272n13.7 | ttf1.1 | | | | | | | | | | | | | | | |
| PI3 kinase pathway (P00048) | 2 | foxo3b | gngt2a | | | | | | | | | | | | | | | |
| GABA-B receptor II signaling (P05731) | 2 | gngt2a | si:ch211-272n13.7 | | | | | | | | | | | | | | | |
| Interferon-gamma signaling pathway (P00035) | 2 | mapk15 | socs3b | | | | | | | | | | | | | | | |
| p53 pathway by glucose deprivation (P04397) | 2 | prkag1 | tp73 | | | | | | | | | | | | | | | |
| Vitamin D metabolism and pathway (P04396) | 2 | fdxr | cyp24a1 | | | | | | | | | | | | | | | |
| Serine glycine biosynthesis (P02776) | 2 | psat1 | phgdh | | | | | | | | | | | | | | | |
| FAS signaling pathway (P00020) | 2 | jun | lmnb1 | | | | | | | | | | | | | | | |
| Angiotensin II-stimulated signaling through G proteins and beta-arrestin (P05911) | 2 | egr1 | gngt2a | | | | | | | | | | | | | | | |
| Circadian clock system (P00015) | 2 | csnk1da | cry3a | | | | | | | | | | | | | | | |
| 5-Hydroxytryptamine degredation (P04372) | 2 | aldh1a2 | aldh3a2b | | | | | | | | | | | | | | | |
| Pyridoxal-5-phosphate biosynthesis (P02759) | 1 | psat1 | | | | | | | | | | | | | | | | |
| Ornithine degradation (P02758) | 1 | azin1b | | | | | | | | | | | | | | | | |
| Adrenaline and noradrenaline biosynthesis (P00001) | 1 | vamp2 | | | | | | | | | | | | | | | | |
| Glutamine glutamate conversion (P02745) | 1 | lgsn | | | | | | | | | | | | | | | | |
| Formyltetrahydroformate biosynthesis (P02743) | 1 | dhfr | | | | | | | | | | | | | | | | |
| Tetrahydrofolate biosynthesis (P02742) | 1 | dhfr | | | | | | | | | | | | | | | | |
| De novo pyrimidine deoxyribonucleotide biosynthesis (P02739) | 1 | rrm2 | | | | | | | | | | | | | | | | |
| De novo purine biosynthesis (P02738) | 1 | rrm2 | | | | | | | | | | | | | | | | |
| Synaptic vesicle trafficking (P05734) | 1 | vamp2 | | | | | | | | | | | | | | | | |
| Endogenous cannabinoid signaling (P05730) | 1 | gngt2a | | | | | | | | | | | | | | | | |
| Xanthine and guanine salvage pathway (P02788) | 1 | pnp5b | | | | | | | | | | | | | | | | |
| Adenine and hypoxanthine salvage pathway (P02723) | 1 | pnp5b | | | | | | | | | | | | | | | | |
| Vitamin B6 metabolism (P02787) | 1 | psat1 | | | | | | | | | | | | | | | | |
| Hypoxia response via HIF activation (P00030) | 1 | hif1ab | | | | | | | | | | | | | | | | |
| Thiamin metabolism (P02780) | 1 | tpk2 | | | | | | | | | | | | | | | | |
| P53 pathway feedback loops 1 (P04392) | 1 | tp73 | | | | | | | | | | | | | | | | |
| General transcription regulation (P00023) | 1 | ttf1.1 | | | | | | | | | | | | | | | | |
| General transcription by RNA polymerase I (P00022) | 1 | ttf1.1 | | | | | | | | | | | | | | | | |
| Nicotine pharmacodynamics pathway (P06587) | 1 | ppp1caa | | | | | | | | | | | | | | | | |
| S-adenosylmethionine biosynthesis (P02773) | 1 | mat1a | | | | | | | | | | | | | | | | |
| Pyruvate metabolism (P02772) | 1 | pck1 | | | | | | | | | | | | | | | | |
| Purine metabolism (P02769) | 1 | pnp5b | | | | | | | | | | | | | | | | |
| 5HT3 type receptor mediated signaling pathway (P04375) | 1 | vamp2 | | | | | | | | | | | | | | | | |

**Supplementary Table 2**

DAVID Bioinformatics Pathway Analysis

| Kegg Pathway | No. of Genes | P-value | Genes | | | | | | | | | | | |
|---|---|---|---|---|---|---|---|---|---|---|---|---|---|---|
| Ribosome | 45 | 2.20E-24 | *rpl10* | *rpl10a* | *rpl12* | *rpl13* | *rpl15* | *rpl17* | *rpl19* | *rpl21* | *rpl22* | *rpl23* | *rpl23a* | *rpl24* |
| | | | *rpl32* | *rpl136a* | *rpl38* | *rpl39* | *rpl14* | *rpl15a* | *rpl7* | *rpl8* | *rpl9* | *rps10* | *rps11* | *rps12* |
| | | | *rps18* | *rps19* | *rps24* | *rps25* | *rps26l* | *rps29* | *rps3a* | *rps8a* | *rps9* | *rpsa* | *rplpl2l* | *rplp0* |
| | | | *rpl28* | *rpl29* | *rps15a* | *rps16* | *rplp1* | *uba52* | | | | | | |
| Glutathione metabolism | 8 | 2.50E-02 | *gstp1* | *gsta.1* | *gpx1a* | *gpx8* | *mgst1.2* | *mgst2* | *rrm2* | *rrm2* | | | | |
| Retinol metabolism | 6 | 5.40E-02 | *aldh1a2* | *bco1* | *cyp26c1* | *cyp26b1* | *rdh8a* | *rdh8b* | | | | | | |
| Insulin resistance | 12 | 9.40E-02 | *cpt1ab* | *mgea5* | *nfkbiab* | *nfkbiab* | *pck1* | *pygma* | *prkcg* | *prkag1* | *ppp1caa* | *ppp1r3b* | *ppp1r3cb* | *socs3b* |

**Supplementary Table 3**

Primers for in situ hybridization and RT-qPCR

| Name | Sequence | Gene | Usage | Primer Pair Efficiency (for RT-qPCR) |
|---|---|---|---|---|
| matn1-FP | CACCCGGATCTTTCAAGTGC | *matrilin 1* | in situ hybridization probe synthesis | |
| matn1-RP-T7 | **TAATACGACTCACTATAGGG**ATTTACACACCACGTCCCCA | | in situ hybridization probe synthesis | |
| klf2a-FP | GCAGCAGCTATATACCGGGG | *kruppel like factor 2a* | in situ hybridization probe synthesis | |
| klf2a-RP-T7 | **TAATACGACTCACTATAGGG**AGCCTTCCCAACTGCAATGA | | in situ hybridization probe synthesis | |
| mxra5b-FP | TGGCATCTCCAAACAGGTCC | *matrix remodeling associated 5b* | in situ hybridization probe synthesis | |
| mxra5b-RP-T7 | **TAATACGACTCACTATAGGG**GGCTGGATTAACTTCCGCCT | | in situ hybridization probe synthesis | |
| rpl13a-FP-qPCR | TCTGGAGGACTGTAAGAGGTATGC | *ribosomal protein L13a* | RT-qPCR | 1.86 |
| rpl13a-RP-qPCR | AGACGCACAATCTTGAGAGCAG | | RT-qPCR | |
| matn1-FP-qPCR | CTATGCATCTTGGGAGCTCAA | *matrilin 1* | RT-qPCR | 1.92 |
| matn1-RP-qPCR | ACTTTAACCTGCTCGAACTCAG | | RT-qPCR | |
| klf2a-FP-qPCR | CAGTTACCGTGCAATTCTGTG | *kruppel like factor 2a* | RT-qPCR | 1.94 |
| klf2a-RP-qPCR | CGTTTCTGATGGTAAAAGTGCC | | RT-qPCR | |
| mxra5b-FP-qPCR | AGACGGTGCTTTTCAGGATC | *matrix remodeling associated 5b* | RT-qPCR | 1.91 |
| mxra5b-RP-qPCR | GATGGAGGAGATGTGGTTGTG | | RT-qPCR | |